Palaeoenvironmental turnover across the Cenomanian-Turonian transition in Oued Bahloul, Tunisia: Foraminifera and geochemical proxies

Matías REOLID, Carlos Alberto SÁNCHEZ-QUIÑÓNEZ, Laia ALEGRET, Eustoquio MOLINA

Research Highlights:

Integrated analysis of foraminifera, geochemical proxies, $\delta^{13}C$ and $\delta^{18}O$ > Decreasing diversity and increasing of productivity and redox proxies during OAE2. > Habitat and trophic regimes of planktic foraminiferal fluctuations during OAE2. > Enhanced productivity and poor mixing waters favored eutrophication and OMZ expansion.

1

2 Palaeoenvironmental turnover across the Cenomanian-Turonian transition in Oued

3 Bahloul, Tunisia: Foraminifera and geochemical proxies

4

5 Reolid, M.[1], Sánchez-Quiñónez, C.A.[2], Alegret, L.[3], Molina, E.[3]

6

7 *1 Departamento de Geología, Universidad de Jaén, Campus Las Lagunillas sn, 23071 Jaén,*

8 *Spain*

9 *2 Departamento de Geociencias, Universidad Nacional de Colombia, Bogotá, Carrera 30, nº*

10 *45-03, Colombia*

11 *3 Departamento de Ciencias de la Tierra e IUCA, Universidad de Zaragoza, Pedro Cerbuna*

12 *12, 50009 Zaragoza, Spain*

13

14 ** Corresponding author:* mreolid@ujaen.es

15

16 ABSTRACT

17 The integrated analysis of foraminiferal assemblages, geochemical proxies, and stable isotopes

18 in the Oued Bahloul section (Tunisia) allowed us to reconstruct the environmental turnover

19 across the Cenomanian–Turonian boundary. An increase in palaeoproductivity proxies (P/Ti,

20 U/Al, Sr/Al) and in $\delta^{13}C$ values, and a decrease in foraminiferal diversity and $\delta^{18}O$ values mark

21 the beginning of the Oceanic Anoxic Event 2 (OAE2) at the *Rotalipora cushmani* and

22 *Whiteinella archaeocretacea* biozones boundary. Eutrophic conditions at the seafloor and in the

23 water column are evidenced by high proportions of buliminids and the replacement of planktic

24 oligotrophic specialist *Rotalipora* by eutrophic opportunist *Hedbergella*. The enrichment in

25 organic matter and redox sensitive elements, together with the abundance of low-oxygen

26 tolerant benthic foraminifera, indicate dysoxic conditions in the deep-water column and at the

27 seafloor (higher U_{aut} than Mo_{aut}). Among planktic foraminifera, deep- and intermediate-dwellers

28 disappear (*Rotalipora* and *Globigerinelloides*), and surface-dwellers proliferate (*Hedbergella*).

29 The persistency of the poorly oxygenated conditions during the *W. archaeocretacea* Biozone

30 locally produced euxinic conditions where Mo_{EF} and Mo_{aut} reach high values, diversity presents

31 minimum values, and benthic foraminifera temporarily disappear. The maximum percentage of

32 heterohelicids indicates a stratified water column with a well-developed oxygen minimum zone.

33 Improved oxygen conditions returned in the upper part of the *W. archaeocretacea* Biozone and

34 *Helvetoglobotruncana helvetica* Biozone, with a slow recovery of foraminiferal assemblages,

35 decrease in eutrophic genera (*Heterohelix*) and increase in mesotrophic genera (*Whiteinella*). A

36 gradual increase in $\delta^{18}O$ values suggests decreased temperatures in surface waters. The OAE2

37 has been attributed to global temperature changes and palaeoceanographic reorganization. The

38 poor mixing of surface and deep waters and enhanced primary productivity related to global

39 warming —associated with increasing continental weathering and nutrient runoff— may have

40 favored the eutrophication of the ocean and the expansion of the oxygen minimum zone.

41

42 Keywords: trophic conditions, redox conditions, ecostratigraphy, foraminifera, OAE2,

43 Cretaceous

44

45 **1. Introduction**

46

47   The Oceanic Anoxic Event 2 (OAE2), also called Bonarelli Event (e.g., Schlanger and

48 Jenkyns, 1976; Arthur et al., 1990), is represented by the worldwide deposition of organic-rich

49 facies close to the Cenomanian–Turonian (C-T) boundary. Two main hypotheses have been

50 invoked to explain the deposition of organic-rich facies during the Cretaceous: (1) oceanic

51 anoxia prevented the degradation of organic matter settling through the water column down to

52 the seafloor by decreased oxygen supply to the deep ocean due to slower oceanic circulation

53 (e.g. Erbacher et al., 2001; Tsandev and Slomp, 2009), or (2) enhanced surface water

54   productivity exceeded the oxygen availability for decaying organic matter at the seafloor (e.g.

55   Sarmiento et al., 1988; Handoh and Lenton, 2003). The OAE2 has been related to

56   palaeoceanographic and climatic changes including greenhouse warming (e.g. Huber et al.,

57   2002; Norris et al., 2002; Bornemann et al., 2008; Tsandev and Slomp, 2009; Monteiro et al.,

58   2012; Pogge von Strandmann et al., 2013), a sea-level transgression (Hallam, 1992), a

59   perturbation of the carbon cycle (e.g. Kuypers et al., 2002; Erba, 2004; Pogge von Strandmann

60   et al., 2013) and a probable massive magmatic episode (e.g. Kuroda et al., 2007; Turgeon and

61   Creaser, 2008; Erba et al., 2013). The planktic foraminiferal turnover (Coccioni and Luciani,

62   2004; Caron et al., 2006) includes the disappearance of genus *Rotalipora* close to the OAE2

63   (e.g. Hart 1996, 1999; Nederbragt and Fiorentino, 1999; Keller et al., 2001; Coccioni and

64   Luciani, 2004). Planktic foraminifera are sensitive to temperature, chemical and trophic

65   conditions of the sea water (Caron, 1983; Caron and Homewood, 1983; Petrizzo, 2002;

66   Gebhardt et al., 2004, 2010), and the ecostratigraphic analysis of their assemblages may be used

67   to reconstruct palaeoceanographic and palaeoecological changes across the OAE2. In addition,

68   the ecostratigraphic analysis of benthic foraminiferal assemblages is a useful tool to interpret

69   fluctuations in oxygen and nutrient availability (e.g. Bernhard, 1986; Nagy, 1992; Jorissen et al.,

70   1995; Van der Zwaan et al., 1999; Klein and Mutterlose, 2001; Reolid et al., 2008, 2012a, b).

71   Some authors have interpreted an extinction event affecting benthic foraminiferal assemblages

72   at the C-T boundary (e.g. Peryt and Lamolda, 1996; Kaiho, 1994, 1999; Peryt, 2004), yet there

73   is no unanimity (Holbourn and Kuhnt, 2002).

74   The analysis of redox-sensitive trace elements (such as Co, Cr, Cu, Mo, and Ni, among

75   others) has proven to be a powerful tool for interpreting redox conditions in oceans during

76   anoxic events. These elements are less soluble under reducing conditions, resulting in

77   synsedimentary enrichments under oxygen-depleted conditions (Wignall and Myers, 1988;

78   Calvert and Pedersen, 1993; Jones and Manning, 1994; Powell et al., 2003; Gallego-Torres et

79   al., 2007; Reolid et al., 2012a, b). Geochemical proxies have also been successfully applied to

80   interpret palaeoproductivity, the most extensively used being Ba/Al, Sr/Al, Ca/Al and P/Ti

81   ratios (e.g., Turgeon and Brumsack, 2006; Gallego-Torres et al., 2007; Robertson and Filippelli,

82   2008; Sun et al., 2008; Reolid and Martínez-Ruiz, 2012; Reolid et al., 2012a, b). The total

83   organic carbon (TOC) has also been employed as an indirect palaeoproductivity proxy (e.g.,

84   Gupta and Kawahata, 2006; Su et al., 2008), although enhanced TOC contents may result from

85   low bottom-water ventilation and oxygen depletion.

86   The aim of this work is to integrate planktic and benthic foraminiferal assemblages and

87   geochemical proxies to determine the palaeoenvironmental turnover across the OAE2 in the

88   Oued Bahloul section, Tunisia. The OAE2 and the C-T transition are recorded in the Bahloul

89   Formation, where numerous studies on microfacies, planktic foraminifera, organic matter and

90   stable isotopes have been carried out (e.g. Caron et al., 1999, 2006; Accarie et al., 2000;

91   Amédro et al., 2005; Zagrarni et al., 2008; Negra et al., 2011; Soua et al., 2011; for recent

92   works). Here we present the first integrated analysis of foraminiferal assemblages and

93   geochemical proxies across the C–T transition at Oued Bahloul.

94

95   **2. Geological setting and the Oued Bahloul section**

96

97   The Cretaceous palaeogeography of Tunisia consists of three main domains: the

98   Saharan Platform in the South, the Central Tunisian Platform, and the Tunisian Basin in the

99   North (Burollet and Busson, 1983). The Central Tunisian Platform was mainly occupied by

100   outer shelf facies rich in planktic foraminifera during the C-T interval. The Bahloul Formation

101   is a widespread wedge that ranges from 23 m thick in the North to 2 m thick in the South, upon

102   the Cenomanian Central Tunisian Platform (Saïdi et al., 1997; Scott, 2003; Robaszynski et al.,

103   2010; Zaghbib-Turki and Soua, 2013; Fig. 1).

104   The Oued Bahloul section was proposed by Burollet (1956) as the type locality of the

105   Bahloul Formation. This outcrop presents the best sedimentary record of the OAE2 in the

106   southern margin of the Tethys (Robaszynski et al., 1993; Caron et al., 2006). The OAE2 is

107   marked by a strong positive shift in $\delta^{13}C$ in bulk carbonate and an increase in organic matter

108   content in the Bahloul Formation (Accarie et al., 1996; Nederbragt and Fiorentino, 1999). The

109   studied interval is 47 m thick and includes the uppermost 5 m of the Fahdène Formation, the

110   Bahloul Formation (29 m thick) and the lowermost 13 m of the Kef Formation (Fig. 1). The

111   Fahdène Formation consists of an alternation of grey-greenish marls and light-coloured

112   limestones. The Bahloul Formation is divided into two members: lower Pre-Bahloul Member

113   and upper Bahloul *s*. *str*. Member (Fig. 1). In turn, the Pre-Bahloul Member is 3.4 m thick and

114   its lower boundary with the Fahdène Formation is sharp and erosive. The first level (0.5 m

115   thick) is a sandy micro-conglomeratic limestone that contains phosphatic black pebbles and

116   quartz grains with well-developed graded bedding. The overlying bed is a bioclastic-rich

117   calcarenite. The upper part of the Pre-Bahloul Member consists of marls with a decreasing

118   content of quartz and bioclasts.

119   The Bahloul *s*. *str*. Member, in this work Bahloul Member, is composed of an

120   alternation of 2 to 5 cm thick, bedded black limestones with thin parallel lamination, and grey

121   marls. Different calcareous packages (50 cm thick) may be recognized where thin black

122   limestones dominate versus intervals with dominance of grey marls. The lamination of the black

123   limestones consists of clear laminae with abundant planktic foraminifera, and black laminae

124   with abundant pellets embedded in a dark matrix with common radiolaria, benthic foraminifera

125   (buliminids) and planktic foraminifera. The vertical transition from laminated black limestones

126   to grey marls is gradual, but the transition from grey marls to black laminated limestones is

127   abrupt. The top of the Bahloul Formation corresponds to densely bioturbated grey marls, and is

128   locally overlain by a thin limestone layer rich in ammonoid moulds with phosphate and

129   glauconite grains (Caron et al., 2006; Zagrarni et al., 2008). The overlying Annaba Member of

130   the Kef Formation consists of grey marls with interlayered marly-limestones.

131   Robaszynski et al. (1990, 1993) located a sequence boundary at the top of Fahdène

132   Formation, at the base of a channel-fill limestone bed (Ce SB5 *s*. Hardenbol et al., 1998). These

133   authors situated the transgressive contact (Ce TS5) at the top of a thicker limestone bed, and the

134   maximum flooding surface between the black laminated limestones of the Bahloul Formation

135   and the marls of the Kef Formation.

136

137   **3. Material and methods**

138

139   Foraminiferal and geochemical analyses were conducted across the upper Cenomanian-

140   lower Turonian at Oued Bahloul section. A total of 25 sampling levels were selected from this

141   47 m thick limestone and marly-limestone succession (Fig. 1). Micropalaeontological samples

142   were disaggregated in water with diluted H_2O_2, washed through a 63 µm sieve, and dried at

143   50ºC. More endurated limestones were immersed in acetic acid (80%) during 1 h to 4 h,

144   depending on the carbonate content, then washed through a 63 µm sieve, and dried at 50ºC.

145   Quantitative studies (Tables 1 and 2) were based on representative splits (using a

146   modified Otto microsplitter) of over 300 specimens of benthic foraminifera larger than 63 µm

147   and 300 specimens of planktic foraminifera larger than 100 µm per sample. The remaining

148   residue was scanned for rare species. Planktic foraminiferal taxa (Fig. 2) were also allocated to

149   biserial (*Heterohelix*), triserial (*Guembelitria*), planispiral (*Globigerinelloides*), and trochospiral

150   morphogroups (Table 3). The latter include strongly keeled (*Dicarinella*, *Rotalipora*,

151   *Thalmanninella*), weakly keeled (*Anaticinella*, *Helvetoglobotruncana*, *Praeglobotruncana*) and

152   unkeeled (*Hedbergella*, *Schackoina, Whiteinella*) forms (Table 3). Changes in depth

153   stratification of the water column and trophic structure, temperature and salinity are the main

154   factors controlling the composition of planktic foraminiferal assemblages. The stratification and

155   richness of nutrients in the water column is narrowly related to productivity and the behavior of

156   the planktic foraminifera. In this sense, opportunists (r-strategists) flourish in eutrophic waters

157   whereas specialists (K-strategists) proliferate in oligotrophic waters (Valentine, 1973). Depth

158   stratification favored differentiation of biotic and abiotic environmental features providing

159   distinct ecological niches and minimizing the competition among species (Hemleben et al.,

160   1989). Based on morphotype analyses (e.g. Corliss, 1985; Jones and Charnock, 1985; Corliss

161   and Chen, 1988), benthic foraminiferal taxa (Fig. 3) were allocated to infaunal, epifaunal, and

162   epifaunal/infaunal morphogroups. In general, benthic foraminifera with trochospiral,

163   planoconvex or biconvex tests are inferred to have had an epifaunal mode of life, living at the

164   sediment surface or in its upper few centimetres, while infaunal foraminifera have cylindrical or

165   flattened tapered, spherical, globular unilocular or elongated multilocular tests, and live in the

166   deeper layers of the sediment (Corliss, 1991; Reolid et al., 2008). Simple diversity (number of

167   species) and the Fisher-α diversity index (e.g. Murray, 1991) were calculated separately for

168   benthic and planktic foraminiferal assemblages.

169   Whole-rock analyses of major elements were carried out in 25 samples using X-ray

170   fluorescence (XRF) in a Philips PW 1040/10 spectrometer. The content of trace elements was

171   determined using an inductively coupled plasma-mass spectrometer (ICP-MS Perkin Elmer

172   Sciex-Elan 5000) at the Centro de Instrumentación Científica (CIC, Universidad de Granada).

173   Instrumental error was $\pm$ 2% and $\pm$ 5% for respective elemental concentrations of 50 ppm and 5

174   ppm.

175   The contents in C, N and S, as well as the total organic carbon (TOC) content, were

176   analysed analyzed with an Elemental Analyzer LECO CNS-TruSpec and an Inorganic Carbon

177   Analyzer CM5240 UIC in the laboratories of the Centro Andaluz de Medio Ambiente

178   (CEAMA, Granada). Total organic carbon was obtained as the difference between total carbon

179   and total inorganic carbon; it was measured in mg and calculated as percentage of sample

180   weight.

181   For δ^{13}C and δ^{18}O analyses, and after roasting, the samples were reacted at 73ºC in an

182   automated carbonate reaction system (Kiel-IV) coupled directly to the inlet of a Finnigan MAT

183   253 gas ratio mass spectrometer at the Laboratory of Stable Isotopes of the University of

184   Michigan. Isotopic ratios were corrected for ^{17}O contribution and are reported in per mil

185   notation relative to the VPDB standard. Values were calibrated using NBS 19 as the primary

186   standard, and analytical precision was monitored by daily analyses of NBS powdered carbonate

187   standards. The measured precision was maintained above 0.02‰ for δ^{13}C and δ^{18}O.

188   In order to compare trace-element proportions in samples with varying carbonate and

189   clay contents, trace-element concentrations were normalized to aluminium content (Calvert and

190   Pedersen, 1993). This technique avoids any lithological effects on trace or major element

191   concentrations, assuming that Al content in sediments is heightened by alumino-silicates (e.g.,

192   Calvert, 1990). The study of palaeoproductivity was carried out applying a set of proxies (Sr/Al,

193   U/Al and P/Ti). To analyzse palaeo-oxygenation, diverse redox proxies evaluating the relative

194   increase of redox sensitive elements (Co/Al, Cr/Al, Cu/Al, Mo/Al, Ni/Al, and Th/Al) were

195   applied throughout the section. Distinct enrichment factors (Mo and U), applied according to

196   Zhou et al. (2012) and Tribovillard et al. (2012), included $Mo_{EF}= [Mo/Al]_{sample}/[Mo/Al]_{PAAS}$ and

197    $U_{EF}= [U/Al]_{sample}/[U/Al]_{PAAS}$. The authigenic values of U and Mo were also calculated according

198   to Zhou et al. (2012), as $Mo_{aut}=[Mo]_{sample}-[Mo]_{PAAS}/[Al]_{PAAS}*[Al]_{simple}$, $U_{aut}=[U]_{sample}-$

199    $[U]_{PAAS}/[Al]_{PAAS}*[Al]_{simple}$.

200

201   **4. Results**

202

203   *4.1. Planktic foraminifera and biostratigraphy*

204

205   Planktic foraminifera dominate the assemblages in the Fahdène Formation (Fig. 4),

206   where the P/B ratio is high (up to 93%). P/B values gradually decrease from the uppermost part

207   of this formation towards the Bahloul Formation, with values commonly <30%, then gradually

208   increase up to 98% towards the middle part of the Bahloul Formation (metre 17), remaining low

209   (<30%) throughout the rest of the section and slightly increasing (up to 57%) in the lower part

210   of the Kef Formation (Fig. 4).

211   A total of 13 genera and 31 species of planktic foraminifera were identified at Oued

212   Bahloul (Fig. 2, Appendix 1). The species distribution allowed us to identify the *Rotalipora*

213   *cushmani, Whiteinella archaeocretacea* and *Helvetoglobotruncana helvetica* biozones (Fig. 5).

214   The upper Cenomanian *R. cushmani* Biozone corresponds to the lower part of the studied

215   interval, and is mostly represented by the Fahdène Formation (Fig. 5). This interval contains

216   abundant keeled trochospiral forms, such as *Rotalipora cushmani*, *Thalmanninella*

217   *greenhornensis*, *Thalmannninella brotzeni*, *Rotalipora monsalvensis* and *Anaticinella*

218   *multiloculata* (with a poorly developed keel). The *W. archaeocretacea* Biozone is 28 m thick,

219   and it includes the uppermost 50 cm of the Fahdène Formation and the Bahloul Formation,

220   containing the Cenomanian-Turonian boundary. This biozone is characterised by common

221   biserial forms such as *Heterohelix reussi* and unkeeled trochospiral forms such as *Whiteinella*

222   *archaeocretacea, Whiteinella aprica*, *Hedbergella planispira* and *Hedbergella delrioensis*. The

223   *H. helvetica* Biozone (lower Turonian) is represented in the uppermost 1.2 m of the Bahloul

224   Formation and in the Kef Formation. This biozone is characterised by the species

225   *Helvetoglobotruncana helvetica*, *Dicarinella imbricata, Shackoina bicornis* and *Whiteinella*

226   *paradubia*.

227   The correlation of the planktic foraminiferal and ammonite (Caron et al., 1999, 2006;

228   Amédro et al., 2005) biozones is shown in Fig. 1C. The record of *Pseudocalycoceras*

229   *angolaense* in the Pre-Bahloul Member and lowermost 3 m of the Bahloul Member indicates the

230   *Metoicoceras geslinianum* Biozone (Cenomanian). The record of *Pseudaspidoceras*

231   *pseudonodosoides* in the Bahloul Formation (12 to 29 m) indicates a late Cenomanian age (*P.*

232   *pseudonodosoides* Biozone), and the record of *Watinoceras* and *Fagesia* in the topmost Bahloul

233   Formation indicates early Turonian age (*Watinoceras* Biozone) (Fig. 1C). The base of the Kef

234   Formation is lower Turonian in age: the *Pseudaspidoceras flexuosum* Biozone has been inferred

235   by correlation with other sections (Accarie et al., 2000), and the *Thomasites rollandi* Biozone is

236   indicated by the record of *Thomasites* sp. (Caron et al., 2006).

237   Diversity of planktic foraminiferal assemblages (Fig. 4) shows a decreasing trend from

238   the Fahdène Formation towards the lower half of the Bahloul Formation (uppermost part of the

239   *R. cushmani* Biozone and lower part of the *W. archaeocretacea* Biozone). Some taxa went

240   extinct (e.g., *Globigerinelloides ultramicrus, Thalmanninella brotzeni, T. greenhornensis,*

241   *Rotalipora cushmani, R. monsalvensis*), and others (e.g. *Anaticinella multicostata, Dicarinella*

242 spp., *Globigerinelloides bentonensis*, *Schackoina* spp.) temporarily disappeared across this

243 interval and reappeared within the upper half of the *W. archaeocretacea* Biozone. Assemblages

244 diversified towards the top of the section, where diversity values are similar to those in the

245 Fahdène Formation (Fig. 4).

246   Assemblages from the lowermost part of the section include common to abundant

247 planispiral (*Globigerinelloides bentonensis*), trochospiral (*Hedbergella delrioensis, H.*

248 *planispira, H. simplex*) and biserial forms (*Heterohelix reussi*) (Fig. 5). Right at the base of the

249 *Whiteinella archaeocretacea* Biozone, the abundance of *H. delrioensis* increases up to 67% of

250 the assemblage (metre 7), and minor quantitative peaks in *Thalmanninella brotzeni* and

251 *Whiteinella aprica* are observed (Fig. 5). Assemblages from the lower half of the Bahloul

252 Formation are strongly dominated by *Heterohelix reussi* (up to 78% of the assemblage), whose

253 relative abundance decreases towards the upper half of this formation, where trochospiral taxa

254 (e.g., *W. archaeocretacea, W. aprica*, *W. baltica*) become common to abundant. Assemblages

255 from the Kef Formation are similar to those from the upper Bahloul Formation, but they contain

256 higher percentages of triserial (*Guembelitria cenomama*), trochospiral (*Hedbergella delrioensis*)

257 and biserial morphogroups (e.g, *Globoheterohelix paraglobulosa*). A 5 m thick interval in the

258 Kef Formation (metres 37–42) is strongly dominated by *W. aprica,* which is rapidly replaced by

259 *Heterohelix reussi* in the uppermost part of the studied section (Fig. 5).

260

261 *4.2. Benthic foraminifera*

262

263   Among benthic foraminifera, calcareous taxa dominate over agglutinated ones. A total

264 of 45 genera and 70 species were recorded throughout the Oued Bahloul section (Appendix 2).

265 *Neobulimina*, *Gavelinella*, *Praebulimina*, *Tappanina*, and *Lenticulina* are the most common

266 genera. *Trochammina*, *Gyroidinoides* and *Laevidentalina* are locally abundant (Fig. 6).

267   Changes in diversity of benthic foraminiferal assemblages are similar to those of

268 planktic assemblages, showing a decreasing trend from the Fahdéne Formation to the middle

269   part of the Bahloul Formation, with minimum values in metres 10–17, and gradual recovery

270   above this interval towards the top of the section (Fig. 4). Sample 17 (Bahloul Formation) is

271   barren of benthic foraminifera (Fig. 6), and very few specimens were found in samples OB-28,

272   OB-30, OB-37, OB-38 and OB-40; thus the benthic foraminiferal counts are not considered as

273   representative in these samples. While planktic foraminiferal assemblages from the uppermost

274   part of the studied section (upper part of *W. archaeocretacea* Biozone and *H. helvetica* Biozone)

275   reach diversity values similar to those in the Fahdéne Formation, the diversity of benthic

276   foraminifera does not fully recover and is significantly lower at the top of the section.

277   Benthic foraminiferal assemblages from the lowermost part of the section are diverse

278   and dominated by epifaunal trochospiral forms (e.g., *Gavelinella flandrini, Gyroidinoides*

279   *globosus* and *Gyroidinoides lenticulus*). Spherical (*Trochammina globolaevigata*) and

280   cylindrical tapered morphogroups (*Praebulimina reussi* and *Laevidentalina* spp.) are also

281   common. The relative abundance of *Gavelinella* spp. significantly increases to the top of Pre-

282   Bahloul Member (Fig. 6), and assemblages are clearly dominated by *Gavelinella* spp.,

283   *Lenticulina gaultina*, and abundant *Globorotalites* spp. (Fig. 6).

284   The boundary between the Pre-Bahloul Member and the Bahloul Member (lower part of

285   the *W. archaeocretacea* Biozone) is characterised by an abrupt decrease in the relative

286   abundance of *Gavelinella* and *Lenticulina,* the disappearance of such taxa as *Trochammina* sp.,

287   *Globorotalites* spp. and *Lingulogavelinella frankei*, and the temporary disappearance of

288   *Laevidentalina* spp., *Laevidentalina gaultina* and *Lenticulina subgaultina* (Lazarus taxa). This

289   boundary marks a clear change in benthic assemblages, from epifauna-dominated assemblages

290   in the lower part of the section to infauna-dominated assemblages in the rest of the studied

291   section. Low-diversity assemblages from the lower half of the Bahloul Member are clearly

292   dominated by *Neobulimina albertensis* (up to 81% of the assemblages), with a minor

293   contribution of *Tappanina laciniosa* and *Coryphostoma* spp. The upper part of this member

294   contains more diversified assemblages, with abundant *Neobulimina albertensis* and *T. laciniosa*,

295   common *Laevidentalina* spp., and new taxa such as *Gavelinella rochardensis* and *Bolivina* sp.

296   (Fig. 6).

297   The lowermost 2.5 m of the *H. helvetica* Biozone are characterised by the disappearance

298   of *Astacolus* spp. and *Dorothia* spp. The Annaba Formation (*H. helvetica* Biozone) contains

299   highly variable percentages of *Neobulimina albertensis* and quantitative peaks of infaunal

300   (*Lenticulina subgaultina*, *Bolivina* spp.) and some epifaunal taxa (*Gavelinella* spp.,

301   *Gyroidinoides lenticulus*).

302

303   *4.3. Geochemistry*

304

305   *4.3.1. Redox proxies*

306   The stratigraphic distribution throughout the succession of the analysed ratios shows

307   three intervals with main changes: a) the base of the *W. archaeocretacea* Biozone, b) the middle

308   part of the *W. archaeocretacea* Biozone, and c) the *W. archaeocretacea*/*H. helvetica* biozone

309   boundary.

310   The lowermost part of the section (*R. cushmani* Biozone) is characterised by decreasing

311   Co/Al, Ni/Al and Th/Al ratios, followed by a sudden increase in all the studied proxies in the

312   Pre-Bahloul Member (base of *W. archaeocretacea* Biozone, Fig. 7). The Mo_{EF}, $Mo_{aut.}$, U_{EF} and

313    $U_{aut.}$ ratios also increase in the Pre-Bahloul Member, with a dramatic increase in U proxies in

314   the topmost Fahdène Formation (*R. cushmani*/*W. archaeocretacea* biozone boundary),

315   immediately preceding the peaks of all other proxies. The U_{EF} values reach 8.08, which is very

316   relevant (Fig. 7). According to Tribovillard et al. (2012), values of elemental enrichment factor

317   > 3 are considerable and > 10 is considered as a strong enrichment.

318   An increase in the Cr/Al ratio and in Mo_{EF} and Mo_{aut} values, and a minor increase in

319   Cu/Al, Ni/Al, U_{EF} and U_{aut} are recorded in sample OB-17 (metre 17, middle part of the *W.*

320   *archaeocretacea* Biozone), which is barren of benthic foraminifera (Fig. 7).

321   The Th/Al ratio remains constant throughout the rest of the section, while the other

322   proxies increase towards the top of the Bahloul Formation (*W. archaeocretacea*/*H. helvetica*

323   biozone boundary), where new peaks in Co/Al, Cr/Al, Cu/Al, Ni/Al and Mo_{EF} and minor

324   increases in Th/Al, $Mo_{aut.}$, U_{EF} and U_{aut} are observed (Fig. 7). Towards the top of the section

325   (Annaba Member), the selected ratios return to the original values recorded in the lowermost

326   part of the section (Fahdène Formation).

327

328   *4.3.2. Palaeoproductivity proxies and TOC*

329   In contrast to redox proxies, the selected palaeoproductivity proxies and TOC only

330   show prominent changes in the Pre-Bahloul Formation (base of the *W. archaeocretacea*

331   Biozone; Fig. 8). The U/Al and P/Ti ratios increase coinciding with the first peak in redox

332   proxies, whereas TOC reaches the maximum values (2.8 wt.%) 1 m above the U/Al and P/Ti

333   peaks. TOC values fluctuate throughout the rest of the section but never exceed the high values

334   recorded at the top of the Pre-Bahloul Formation. The Sr/Al ratio and TOC values (2.1 wt.%)

335   are higher in the *W. archaeocretacea*/*H. helvetica* biozone boundary than in the other biozones.

336   Apart from decreased TOC and Sr/Al values in the lower half of the Annaba Member,

337   palaeoproductivity proxies remain relatively stable up to the top of the section.

338

339   *4.3.3. $\delta^{13}C$ and $\delta^{18}O$*

340   Bulk rock $\delta^{13}C$ values obtained in this study have been compared to previous results by

341   Caron et al. (2006) and Zagrarni et al. (2008), and show similar trends (Fig. 9). A 2‰ increase

342   (from 1.83 – 3.76‰) in $\delta^{13}C$ is recorded at the transition from the Pre-Bahloul Member to the

343   Bahloul Member (lower part of the *W. archaeocretacea* Biozone). A marked increase in $\delta^{13}C$

344   values is a typical feature of the OAE2 (e.g. Scholle and Arthur, 1980; Schlanger et al., 1987).

345    $\delta^{13}C$ values remain high throughout most of the *W. archaeocretacea* Biozone (mean value

346   3.09‰), and decrease in its uppermost 5 m. The $\delta^{13}C$ mean value in the *H. helvetica* Biozone

347   (base of the Annaba Member) is 2.30‰.

348   The $\delta^{18}O$ values gradually decrease from the Fahdène Formation to the Bahloul Member

349   (from -4.54 to -5.31‰), and remain low (mean value -5.39‰) throughout the rest of the Bahloul

350   Formation, progressively increasing in the Annaba Member (mean value -4.55‰).

351

352   **5. Palaeoenvironmental interpretation**

353

354   *5.1. Top of the Fahdène Formation and Pre-Bahloul Member*

355

356   Analysis of redox conditions in the water column and at the seafloor is based on redox-

357   sensitive trace elements (Co, Cr, Cu, Mo, Ni, U, and Th), which tend to co-precipitate with

358   sulfides (mainly pyrite) and are usually not remobilised during diagenesis in the absence of

359   post-depositional replacement of oxidizing agents (Tribovillard et al., 2006). The enrichment in

360   redox sensitive elements (Co/Al, Cr/Al, Cu/Al, U/Al, Th/Al, Mo_{EF}, Mo_{aut}, U_{EF} and U_{aut}) points

361   to depleted oxygen conditions during deposition of the Pre-Bahloul Member (base of the *W.*

362   *archaeocretacea* Biozone). U-based proxies (U_{EF}=8.08; Fig. 7) and increased TOC values point

363   to depleted oxygen conditions in the lower part of the water column.

364   The P/Ti ratio is a commonly used proxy for productivity (Latimer and Filippelli, 2001;

365   Robertson and Filippelli, 2008; Reolid et al., 2012a, b). Increased values are related to higher

366   phosphorous supply to the seafloor derived from biological processes, not from terrigenous

367   components (Latimer and Filippelli, 2001; Flores et al., 2005; Sen et al., 2008). At Oued

368   Bahloul, the increase in P/Ti values at the base of the *W. archaeocretacea* Biozone (Pre-

369   Bahloul Member) indicates an abrupt increase in productivity (Fig. 8). Mort et al. (2007)

370   suggested that the increase in P-accumulation rates coinciding with the OAE2 may be related to

371   an overall increase in surface-water productivity. At Oued Bahloul, high P/Ti values coincide

372   with high U/Al and U_{EF} values (Figs. 7 and 8), and point to a productivity increase in the Pre-

373   Bahloul Member. The Sr/Al ratio, which has also been used as a palaeoproductivity proxy (Sun

374   et al., 2008; Reolid et al., 2012), shows a minor increase in the Pre-Bahloul Member (Fig. 8).

375   This interpretation is compatible with the decreased foraminiferal diversity (both in

376   planktic and benthic assemblages) and with the assemblage turnover at the base of the *W.*

377   *archaeocretacea* Biozone (Figs. 4–6). Among benthic assemblages, the percentage of

378   *Gavelinella* spp. and *Lenticulina* spp. significantly increases in the Pre-Bahloul Member, and

379   *Globorotalites* shows a minor peak (Fig. 6). *Lenticulina* is regarded as an opportunistic genus

380   that recolonizes the seafloor after redox fluctuations (Tyszka, 1994; Reolid et al., 2008; Reolid

381   et al., 2012a). *Gavelinella* spp. is a low-oxygen tolerant genus (Sliter, 1975; Gertsch et al.,

382   2010), and it occurs in shales with high organic matter levels (Holbourn et al., 2001).

383   *Globorotalites* has been observed to peak under stressful conditions at the seafloor after the

384   Cretaceous/Paleogene impact event, mostly related to changes in the type (rather than in the

385   amount) of food supply (Alegret, 2007; Alegret et al., 2012). This assemblage composition,

386   together with the disappearance of some taxa at the *R. cushmani/W. archaeocretacea* biozone

387   boundary, indicate dysoxic conditions and a high food flux to the seafloor. The disappearance

388   of *Dorothia*, *Gyroidinoides*, *Laevidentalina*, *Lingulogavelinella*, and *Pyrulinoides* may be

389   related to the dysoxic conditions in the sea-bottom. The boundary between the Pre-Bahloul

390   Member and the Bahloul Member is characterised by the disappearance or abrupt decrease in

391   relative abundance of *Lenticulina*, *Gavelinella* and *Globorotalites*, and by an abrupt increase in

392   low-oxygen tolerant forms such as epifaunal *Neobulimina* (Fig. 6).

393   The planktic foraminiferal turnover across the Pre-Bahloul Member includes the

394   disappearance of specialist, intermediate to deep-dweller species adapted to oligotrophic

395   environments (*Rotalipora monsalvensis*), along with the temporary disappearance of

396   mesotrophic, intermediate-dwellers (*Praeglobotruncana gibba*, *Dicarinella* spp.). A peak in the

397   relative abundance of the specialist intermediate-dweller *Thalmanninella brotzeni* is recorded at

398   the base of the Pre-Bahloul Member just before its disappearance (Fig. 5). The percentages of

399   the eutrophic, surface-dweller species *Hedbergella delrioensis* (and *Whiteinella aprica* to a

400   minor extent) increase towards the top of the Pre-Bahloul Member, coinciding with the peaks in

401   redox proxies (Figs. 7 and 8), the disappearance of deep-dweller species (*R. cuhsmani*), and the

402 temporary disappearance of surface- and intermediate-dwellers (*Globigerinelloides* spp.,

403 *Praeglobotruncana stephani*). These data suggest that the deeper and intermediate layers of the

404 water column were more severely affected than surface waters at the *R. cushmani-W.*

405 *archaeocretacea* biozone transition, as suggested by Coccioni and Luciani (2004). An increase

406 in surface palaeoproductivity is supported by the disappearance of the large keeled *Rotalipora*, a

407 specialist genus probably living at or below the thermocline in oligotrophic conditions

408 (Coccioni and Luciani, 2004; Table 3), and by the increase in relative abundance of small-sized

409 *Hedbergella* and *Heterohelix*, opportunistic taxa adapted to eutrophic conditions (e.g. Hart,

410 1999; Keller et al., 2001; Table 3). An increase in P content in sections from the Tethys and

411 North Atlantic has been interpreted as indicative of changes in continental input (and nutrient

412 influx) or upwelling intensification during the late Cenomanian (Mort et al., 2007). Monteiro et

413 al. (2012) suggested that a high P content could be sustained by increased chemical weathering

414 and P regeneration from anoxic sediments.

415 　　　　The increase in P/Ti and U/Al in the Pre-Bahloul Member has good stratigraphic

416 correlation with increased redox proxies (Co/Al, Cr/Al, Ni/Al, and Th/Al), and shows a short

417 delay with respect to the increase in TOC values (Figs. 7 and 8). The marine anoxia of the

418 OAE2 is thought to have been related to enhanced biological productivity (e.g. Monteiro et al.,

419 2012; Pogge von Strandmann et al., 2013). Uranium and organic matter in the sediment are

420 related, as uranium may form a complex with dissolved fulvic acid in hemipelagic sediments

421 (Nagao and Nakashima, 1992). In this sense, high values for U/Al, U_{EF} and U_{aut} are congruent

422 with the high values of P/Ti.

423 　　　　In open-ocean systems with suboxic bottom waters, U_{aut} enrichment is greater than that

424 of Mo_{aut} because U_{aut} accumulation begins at the Fe(II)-Fe(III) redox boundary (Zhou et al.,

425 2012), while Mo_{aut} accumulation becomes more important as waters become euxinic. Higher

426 values of U_{aut} recorded in the Pre-Bahloul Member are congruent with oxygen-depleted

427 conditions not only at the sea-bottom waters but also in the deeper layers of the water column,

428 where deep dwellers such as *Rotalipora* inhabited. The relative abundance of surface dwellers

429 such as *Hedbergella delrioensis* increased in the Pre-Bahloul Member.

430

431 *5.2. Bahloul* s. str. *Member*

432

433 Two intervals with significant peaks in redox proxies are recorded within the Bahloul

434 Member (Fig. 7). The first one is located in the middle part of this unit (sample OB-17), and the

435 second one is located towards its top, at the *W. archaeocretacea*/H. *helvetica* Biozone boundary

436 (Fig. 7). Some redox proxies, such as Th/Al, U_{EF} and U_{aut}, do not show any significant changes

437 across this interval.

438 In the lower half of the Bahloul Member (previous to sample OB-17), the amount of

439 dissolved oxygen in the sea-bottom waters is interpreted to have been even lower than in the

440 underlying Pre-Bahloul Member, as inferred from the disappearance of several benthic

441 foraminiferal taxa and from the very low-diversity assemblages (Figs. 2 and 6), which are

442 dominated by low-oxygen tolerant forms such as *Neobulimina* (Gertsch et al., 2010),

443 *Praebulimina*, *Coryphostoma* and *Tappanina* spp. (incl. *T. laciniosa*). The clear dominance of

444 *Neobulimina* and *Praebulimina* immediately above the extinction interval suggests that they

445 may have behaved as disaster species, as suggested by Peryt and Lamolda (1996). According to

446 these authors, disaster taxa evolved during the late, most stressful phases of an extinction

447 interval, and persisted during the survival and recovery intervals. Species of *Coryphostoma*

448 have small, tapered tests with abundant pores, and are common in dysaerobic environments

449 (e.g., Leutenegger and Hansen, 1979; Bernhard, 1986). *Coryphostoma* is a common genus in

450 low-oxygen environments during the early Danian (Coccioni et al., 1993; Alegret, 2007), and

451 *Tappanina laciniosa* is a biserial, infaunal species that has been reported from dysoxic facies in

452 highly eutrophic environments (e.g. Eicher and Worstell, 1970; Gustafsson et al., 2003;

453 Friedrich and Erbacher, 2006). Moreover, the dominance of infaunal taxa in the Bahloul

454 Member and in the Annaba Member supports the interpretation of low oxygen conditions at the

455 seafloor (Jorissen et al., 1995).

456   The decreased abundance of the surface-dweller *Hedbergella delrioensis* at the base of

457 the Bahloul Member (Fig. 5) points to oxygen-depleted eutrophic surface waters, while low-

458 oxygen conditions only affected deep and intermediate waters in the underlying Pre-Bahloul

459 Member. Only *Heterohelix reussi* —opportunistic taxon adapted to eutrophic conditions—

460 proliferates in the lower part of Baloul Member in a context of decreasing diversity of planktic

461 foraminiferal assemblages.

462   Relatively higher TOC values (mean 1.42 wt.%) and high $\delta^{13}C$ are recorded in the

463 Bahloul Member (Fig. 8), suggesting higher productivity than in the other units and high

464 accumulation of organic matter derived from surface primary productivity (Schlanger and

465 Jenkyns, 1976; Arthur et al., 1990; Ingall et al., 1993; Van Cappellen and Ingall, 1994; Mort et

466 al., 2007). TOC values have been used as an indirect palaeoproductivity proxy by various

467 authors (e.g., Calvert and Fontugne, 2001; Gupta and Kawahata, 2006; Plewa et al., 2006; Su et

468 al., 2008; Reolid et al., 2012a) when TOC is related to phytodetritus associated with

469 phytoplankton or dinoflagellate remains. Nevertheless, because high TOC values may result

470 from low bottom-water ventilation and oxygen depletion, they are not necessarily related to

471 high surface productivity. According to Tribovillard et al. (2006), the TOC is generally

472 proportional to surface-water productivity and constitutes a useful palaeoproductivity proxy in

473 spite of certain complications attributable to efficient organic recycling, export productivity,

474 delivery to the sediment-water interface and final burial. The maximum TOC values (2.82

475 wt.%) are recorded at the base of this unit (Fig. 8), coeval with high percentages of *Heterohelix*

476 *reussi*, *Heterohelix moremani* and *Hedbergella planispira* (Fig. 5), which are thought to be

477 indicative of eutrophic environments (Table 3). These results are compatible with the analyses

478 of organic matter carried out by Farrimond et al. (1990), who reported abundant algal-derived

479 biological markers across the Cenomanian-Turonian transition at Oued Bahloul, suggesting high

480 surface productivity. High TOC values are also correlated to high percentages of *Neobulimina*

481 and other buliminids (Fig. 6), which are considered to be indicators of high-food and/or low

482 oxygenation at the seafloor in the modern oceans (e.g., Fontanier et al., 2002; Gooday, 2003).

483 The dominance of buliminids is also compatible with the proposed conditions, given that high

484 proportions of buliminids indicate eutrophic conditions (Sprong et al., 2013). These results point

485 to a high export productivity and poor oxygenation at the sea-bottom waters during deposition

486 of the lower part of the Bahloul Member; and combined with the high TOC and $\delta^{13}C$ values

487 (Figs. 8 and 9), they suggest a major climatic and palaeoceanographic perturbation in a

488 transgressive context (e.g. Zagrarni et al., 2008). In addition, Caron et al. (1999) and Soua et al.

489 (2011) documented the proliferation of radiolarians (mainly Nassellarian) and diatoms at the

490 base of the *Whiteinella archaeocretacea* Biozone (from the uppermost Pre-Bahloul Member), in

491 coincidence with an increased abundance of *Heterohelix* during the deposition of dark laminated

492 limestones. These authors interpreted the proliferation of radiolarians as indicative of renewal of

493 nutrient-rich oceanic waters and increase in water depth.

494   An increase in Mo_{EF} and Mo_{aut}, and a minor increase in Cu/Al, Cr/Al and Ni/Al are

495 observed in bed OB-17 (Fig. 7). High Mo_{EF} and Mo_{aut} values require the presence of H_2S

496 (euxinic conditions) (Tribovillard et al., 2012; Zhou et al., 2012). The gradual increase in Mo_{EF}

497 and Mo_{aut} across the lower half of the studied section indicates a progressive decrease in oxygen

498 availability towards euxinic conditions. Other authors have reported euxinic conditions from the

499 OAE2 (e.g. Wang et al., 2001; Scopelliti et al., 2004). The progressive accentuation of oxygen-

500 depleted conditions from the Pre-Bahloul Member towards the lower half of the Bahloul

501 Member is compatible with the disappearance of benthic taxa that flourished at the beginning of

502 the suboxic conditions (e.g., *Lenticulina*, *Gavelinella*, *Globorotalites*), and with the proliferation

503 of the disaster genus *Neobulimina* (low oxygen tolerant form, Friedrich et al., 2009), which has

504 been documented from other sections during the Cenomanian–Turonian event (e.g. Gebhardt et

505 al., 2004). Finally, the interpretation of anoxia/euxinia is compatible with the lack of benthic

506 foraminifera and very low diversity of planktic assemblages in sample OB-17. The bed OB-17

507 represents a benthic barren level. Unfavorable conditions also affected the water column during

508   this interval, as inferred from the dramatic decrease in the percentage of the opportunistic

509   surface dweller *Hedbergella delrioensis* and the increase in opportunistic surface to

510   intermediate dwellers (*Heterohelix* spp.). The highest relative abundances of heterohelicids (*H.*

511   *reussi*) occur in OB-17 (Fig. 5), where maximum values of Mo_{EF} and Mo_{aut} are recorded (Fig.

512   7). *Heterohelix* has been interpreted as a low-oxygen tolerant genus that bloomed in stratified

513   open marine settings with a well-developed oxygen minimum zone (e.g. Leckie et al., 1998;

514   Premoli Silva and Sliter, 1999; Keller et al., 2001; Keller and Pardo, 2004).

515   Redox proxies indicate the return to normal oxygen conditions across the upper half of

516   the Bahloul Member, but the palaeoenvironmental perturbation induced slow recovery of the

517   foraminiferal assemblages, as reflected by the dominance of the opportunistic *Heterohelix* and

518   *Whiteinella* in intermediate and surface waters, respectively. Diversity of benthic assemblages

519   slightly increases through this interval, and assemblages are dominated by buliminids

520   (*Neobulimina* and *Praebulimina*), with higher percentages of *Gavelinella rochardensis,*

521   *Laevidentalina* and *T. laciniosa* towards the upper part of the Bahloul Formation. The species *T.*

522   *laciniosa* and the genera *Gavelinella*, *Neobulimina* and *Praebulimina* have been reported from

523   dysoxic facies in highly eutrophic environments and high organic-matter fluxes (e.g. Eicher and

524   Worstell, 1970; Coccioni et al., 1993; Gustafsson et al., 2003; Gebhardt et al., 2004; Friedrich

525   and Erbacher, 2006; Friedrich et al., 2009). This assemblage suggests that the repopulation

526   phase at the seafloor occurred in the upper half of the Bahloul Formation. Among planktic

527   foraminifera, the opportunistic surface dweller *Whiteinella* proliferated in this interval, together

528   with the intermediate dweller *H. reussi*, as previously reported from the Tethys area (Coccioni

529   and Luciani, 2004). Non-opportunist forms including *Praeglobotruncana* and *Dicarinella* are

530   recorded in the upper part of the *W. archaeocretacea* Biozone, whereas deep dweller specialists

531   as *Rotalipora* are definitively extinct and there are no genera occupying this ecologic niche.

532   A positive peak in redox proxies (Mo_{EF}, Cu/Al, Co/Al, Cr/Al, Ni/Al ratios) and a minor

533   increase in some palaeoproductivity proxies have been recorded at the *W. archaeocretacea*/*H.*

534   *helvetica* biozone boundary (sample OB-33), coinciding with an increase in the percentage of

535   buliminids and *Guembelitria cenomana*. *Guembelitria* is interpreted as an opportunist surface

536   dweller adapted to poorly oxygenated, eutrophic waters (Table 3) or to variable salinity and

537   nutrient levels (Keller and Pardo, 2004). The obtained data indicate high productivity and low-

538   oxygen conditions both in surface waters and at the seafloor towards the top of the *W.*

539   *archaeocretacea* Biozone. According to Soua et al. (2011), the composition of radiolarian

540   assemblages also experiments a turnover related to low-oxygen conditions with a drastic

541   decrease of nassellarians and an abundance and diversification of spumellarians.

542

543   *5.3. Base of the Kef Formation*

544

545   A progressive increase in the diversity of planktic assemblages, together with the co-

546   occurrence of surface and intermediate-to-deep dwellers indicates partial recovery of the

547   assemblages at the beginning of the *H. helvetica* Biozone. The most common taxa (*Whiteinella,*

548   *Heterohelix, Hedbergella*) are indicative of eutrophic, oxygenated to poorly oxygenated surface

549   and intermediate waters. Deep dwellers such as the intermediate to specialist

550   *Helvetoglobotruncana* (Table 3) make only a minor contribution to the assemblages. Just after

551   the last suboxic pulse of the top of Bahloul Member (level OB-33), *Whiteinella* proliferates

552   again in the assemblage as a rapid response to improved conditions.

553   In benthic microhabitats, the beginning of the *H. helvetica* Biozone is marked by an

554   increase in relative abundance of *Gyroidinoides*, *Lenticulina* and *Planularia*, and a decrease in

555   *Tappanina* and *Gavelinella.* Diversity of the benthic assemblages remains low, and the

556   dominance of buliminids (*Praebulimina* and *Neobulimina*) indicates a high food supply or low-

557   oxygen conditions at the seafloor (Jorissen et al., 1995; Widmark and Speijer, 1997; Fontanier

558   et al., 2002).

559

560   **6. Climatic and palaeoceanographic changes across the Cenomanian–Turonian boundary**

561

562   Analyses of $\delta^{18}O$ in bulk rock show a ~ 1.5 ‰ decrease from the base of the section

563   towards the Bahoul Member, followed by a gradual recovery above this unit (Fig. 9). Assuming

564   these results have not been strongly altered by diagenesis, we infer significantly warmer (~ 6ºC)

565   temperatures during deposition of the organic rich facies of the Bahoul Member (*W.*

566   *archaeocretacea* Biozone), coeval with the disappearance of specialist planktic foraminifera

567   (e.g. *Rotalipora*) and with the proliferation of opportunistic, eutrophic forms such as

568   *Heterohelix* and *Hedbergella*. These results suggest a narrow link between the development of

569   the anoxic event and eutrophic conditions with changes in the ocean-atmosphere system. Some

570   authors have identified a short term cooling during the OAE2 (e.g. Jarvis et al., 2011; Gavrilov

571   et al., 2013; Zheng et al., 2013), which we were not able to recognize in our record from Oued

572   Bahloul at the present resolution.

573   In the transgressive context of the Cenomanian–Turonian boundary (e.g. Zagrarni et al.,

574   2008), the enhanced fertility resulting in high primary productivity and eutrophication was

575   favored by nutrient inputs by leaching from flooded shelves (Erbacher et al., 2001) or enhanced

576   continental supply of nutrients (Föllmi, 1995; Handoh and Lenton, 2003). According to Wagner

577   et al. (2007), the warm humid climate contributes to an intensified hydrological cycle and

578   enhanced export of nutrient-rich weathered material from land to the ocean, as also suggested

579   for the Paleocene-Eocene Thermal Maximum (see refs. in Arreguín-Rodríguez et al., 2014). For

580   the end of Cenomanian, another hypothesis was developed by Caron et al. (1999): the

581   alternation of climatic fluctuations, with evaporation/precipitation in low latitude areas and the

582   formation of dense, hypersaline sea waters.

583   Calcareous nannofossil turnover has been interpreted in terms of enhanced fertility and

584   increased temperatures, pointing to an eutrophication event (Erba, 2004; Hardas and Mutterlose,

585   2007). P-cycling models for Cretaceous Anoxic Events, however, indicate that enhanced

586   primary productivity is not enough for producing anoxic conditions in the bottom waters if

587   water circulation exists (Tsandev and Slomp, 2009). According to these authors, the global

588   ocean has to be sufficiently stagnant (low mixing) to allow the system to achieve oxygen

589 depletion in the deep sea. In general, the thermohaline circulation during the Cretaceous is

590 believed to have been slower due to reduced thermal gradients between the tropics and poles

591 (e.g. Shlanger and Jenkyns, 1976; Fischer and Arthur, 1977), and the wider extension of

592 continental shelves (e.g. Bjerrum et al., 2006). In this context, increased P supply from flooded

593 shelves and weathered continental areas may have triggered enhanced primary production and

594 anoxia in a stagnant ocean. In the Oued Bahloul section, a significant increase in P has been

595 observed in the Pre-Bahloul Member coeval with high dominance of *Hedbergella* and the

596 extinction of *Rotalipora*. The progressive decrease in oxygenation of bottom- and deep-waters

597 towards anoxic conditions in the Bahloul Member (metre 17, OB-17) represents the most

598 stressing conditions for the foraminiferal assemblages, with the disappearance of benthic

599 foraminifera, the expansion of the oxygen minimum zone coincident with maximum values of

600 *Heterohelix,* and probably euxinic conditions in the low water column as indicated by increased

601 Mo_{EF} and $Mo_{aut.}$

602

603 **7. Conclusions**

604

605 The integrated analysis of planktic and benthic foraminiferal assemblages, geochemical

606 proxies, TOC and $\delta^{13}C$ and $\delta^{18}O$ from the classic locality of the Oued Bahloul section allowed

607 us to interpret: (a) the redox and palaeoproductivity fluctuations related to the C/T boundary,

608 and (b) the ecostratigraphic changes of foraminiferal associations across the OAE2.

609 Significant changes were recorded across the *R. cushmani*/*W. archaeocretacea*

610 boundary, and planktic and benthic foraminiferal diversity decreased. The disappearance of the

611 planktic genera *Rotalipora*, *Praeglobotruncana*, *Globigerinelloides* and *Thalmanninella*, and

612 the occurrence of the opportunist genus *Hedbergella*, together with the proliferation of

613 buliminids and the increase in palaeoproductivity proxies (P/Ti, U/Al, Sr/Al), indicate eutrophic

614 conditions both in the water column and at the seafloor. The abundance of low-oxygen tolerant

615 genera of benthic foraminifera at the base of *W. archaeocretacea* Biozone is compatible with

616   the enrichment in redox proxies indicating dysoxic conditions in sediment pore water. Deep

617   waters were also oxygen-depleted, as deduced from higher values of U_{aut} than Mo_{aut}, favouring

618   the disappearance of *Rotalipora* and *Globigerinelloides* and the proliferation of surface-dweller

619   *Hedbergella*. The maximum TOC values registered in the lower part of the *W. archaeocretacea*

620   Biozone indicate an abrupt increase in organic matter coeval with an increase in

621   palaeoproductivity and redox proxies.

622   The persistence of the poorly oxygenated conditions in the *W. archaeocretacea* Biozone

623   probably produced euxinic conditions, as indicated by high Mo_{EF} and Mo_{aut} values, minimum

624   diversity and the local disappearance of benthic forms. The decrease in abundance of

625   opportunist surface dwellers (*Hedbergella*) and the increase in opportunist intermediate dwellers

626   (heterohelicids), together with maximum values of Mo_{EF} and Mo_{aut}, indicate stressed conditions

627   and stratified open marine settings with a well-developed oxygen minimum zone.

628   The redox proxies indicate a return to normal oxygen conditions in the upper part of the

629   *W. archaeocretacea* Biozone, with a slow recovery of foraminiferal assemblages. The genus

630   *Whiteinella*, characteristic of mesotrophic environments, becomes more abundant upward in the

631   section. The subsequent colonization of the bottom after the anoxic event was produced by

632   *Praebulimina* (disaster genus), *Gavelinella*, *Neobulimina* and *Tappanina*. These genera are

633   low-oxygen tolerant and related to high organic matter fluxes, thus representing the

634   repopulation episode of the bottom after the benthic barren interval.

635   The *W. archaeocretacea*/*H. helvetica* biozone boundary is characterized by increasing

636   values of redox proxies, coeval with a new peak of *Praebulimina*, a decrease in *Whiteinella* and

637   the record of opportunist *Guembelitria*.

638   The beginning of the *H. helvetica* Biozone indicates a partial recovery of the planktic

639   foraminiferal assemblage due to a persistent dominance of opportunists (*Whiteinella* and

640   *Hedbergella* in surface waters, and *Heterohelix* in intermediate waters). In benthic

641   microhabitats, the beginning of the *H. helvetica* Biozone is marked by an increase in relative

642   abundance of *Neobulimina*, *Lenticulina*, and *Gyroidinoides,* and a decrease in *Tappanina*.

643　　　　Temperature changes and palaeoceanographic reorganization have been inferred across

644　　the OAE2. This entailed a low mixing of surface and deep waters (poor ocean ventilation) and

645　　enhanced primary productivity related to global warming, increasing continental weathering and

646　　nutrient input to the ocean. The expansion of the oxygen minimum zone and the eutrophication

647　　led to a reduced diversity of foraminifera and the planktic foraminiferal shift, showing a

648　　dominance of genera with low-oxygen tolerance typical of high mesotrophic to eutrophic

649　　conditions.

650

664

665

666　　**References**

667

668　　Accarie, H., Emmanuel, L., Robaszynski, F., Baudin, F., Amédro, F., Caron, M., Deconinck,

669　　　　J.F., 1996. La géochimie isotopique du carbone (δ^{13}C) comme outil stratigraphique.

670   Aplication à la limite Cénomanien/Turonien en Tunisie central. Comptes Rendus

671   Academie des Sciences, Paris 322, 579–586.

672 Accarie, H., Robaszynski, F., Amédro, F., Caron, M., Zagrarni, M.F., 2000. Stratigraphie

673   événementielle au passage Cénomanien-Turonien dans le secteur occidental de la plate-

674   forme de la Tunisie centrale (Formation Bahloul, région de Kalaat Senan). Annales des

675   Mines et de la Geologie, Tunisie 40, 63–80.

676 Alegret, L., 2007. Recovery of the deep-sea floor after the Cretaceous/Paleogene boundary

677   event: the benthic foraminiferal record in the Basque-Cantabrian basin and in South-eastern

678   Spain. Palaeogeography, Palaeoclimatology, Palaeoecology 255, 181–194.

679 Alegret, L., Thomas, E., Lohmann, K.C., 2012. End-Cretaceous marine mass extinction not

680   caused by productivity collapse. Proceedings of the National Academy of Sciences 109,

681   728–732

682 Amédro, F., Accarie, H., Robaszynski, F., 2005. Position de la limite Cénomanien-Turonien

683   dans le Formation Bahloul de Tunisie centrale : apports intégrés des ammonites et des

684   isotopes du carbone (δ^{13}C). Eclogae Geologicae Helvetiae 98, 151–167.

685 Arreguín-Rodríguez, G.J., Alegret, L., Sepúlveda, J., Newman, S., Summons, R. E. 2014.

686   Enhanced terrestrial input supporting the *Glomospira* acme across the Paleocene-Eocene

687   boundary in Southern Spain. Micropaleontology 60, 43–51.

688 Arthur, M.A., Jenkyns, H.C., Brumsack, H.J., Schlanger, S.O., 1990. Stratigraphy,

689   geochemistry, and paleoceanography of organic carbon-rich Cretaceous sequences. In:

690   Ginsburg, R.N., Beaudoin, B., (eds.), Cretaceous Ressources, Events and Rhythms:

691   Background and Plans for Research, NATO ASI series, pp. 75–119.

692 Bernhard, J.M., 1986. Characteristic assemblages and morphologies of benthic foraminifera

693   from anoxic, organic rich deposits: Jurassic trough Holocene. Journal of Foraminiferal

694   Research 16, 207–215.

695 Bjerrum, C.J., Bendtsen, J., Legarth, J.J.F., 2006. Modeling organic carbon burial during sea

696   level rise with reference to the Cretaceous. Geochemistry, Geophysics, Geosystems 7,

697   Q05008.

698 Bornemann, A., Norris, R.D., Friedrich, O., Beckmann, B., Schouten, R., Sinninghe-Damste, J.,

699   Vogel, J., Hofmann, P., Wagner, T., 2008. Isotopic evidence for glaciation during the

700   Cretaceous super-greenhouse. Science 319, 951–954.

701 Burollet, P.F., 1956. Contribution à l'étude stratigraphique de la Tunisie Centrale. Annales des

702   Mines et de la Géologie, Tunisie 18, 1–345.

703 Burollet, P.F., Busson, G., 1983. Plate-forme Saharienne et Mésogée au cours du Crétacé. Notes

704   et Memoires Total-CFP 18, 17–26.

705 Calvert, S.E., 1990, Geochemistry and origin of the Holocene sapropel in the Black Sea. In

706   Ittekkot, V., Kempe, S., Michaelis, W., and Spitzy, A. (eds.), Facets of Modern

707   Biogeochemistry, Springer, Berlin, pp. 326–352.

708 Calvert, S.E., Fontugne, M.R., 2001. On the late Pleistocene-Holocene sapropel record of

709   climatic and oceanographic variability in the eastern Mediterranean. Paleoceanography 16,

710   78–94.

711 Calvert, S.E., Pedersen, T.F., 1993. Geochemistry of recent oxic and anoxic marine sediments:

712   Implications for the geological record. Marine Geology 113, 67–88.

713 Caron, M., 1983. La spéciation chez les Foraminifères planctiques: une réponse adaptée aux

714   contraintes de l´environnement. Zitteliana 10, 671–676.

715 Caron, M., Homewood, P., 1983. Evolution of early planktic foraminifers. Marine

716   Micropaleontology 7, 453–462.

717 Caron, M., Dall'Agnolo, S., Accarie, H., Barrera, E., Kauffman, E.G., Amédro, F.,

718   Robaszynski, F., 2006. High-resolution stratigraphy of the Cenomanian_Turonian

719   boundary interval at Pueblo (USA) and wadi Bahloul (Tunisia): stable isotope and bio-

720   events correlation. Geobios 39, 171–200.

721 Caron, M., Robaszynski, F., Amédro, F., Baudin, F., Deconinck, J.F., Hochli, P., Von Salis-

722   Perch Nielsen, K., Tribovillard, N., 1999. Estimation de la durée de l'événement anoxique

723   global au passage Cénomanien-Turonien. Approche cyclostratigraphique dans la Formation

724   Bahloul en Tunisie centrale. Bulletin de la Société Géologique de France 170, 145–160.

725 Coccioni, R., Fabbrucci, L., Galeotti, S., 1993. Terminal Cretaceous deep-water benthic

726   foraminiferal decimation, survivorship and recovery at Caravaca (SE Spain). Paleopelagos

727   3, 3–24.

728 Coccioni, R., Luciani, V., 2004. Planktonic foraminifera and environmental changes across the

729   Bonarelli Event (OAE2, Latest Cenomanian) in its type area: a high-resolution study from

730   the Tethyan reference Bottaccione section (Gubbio, Central Italy). Journal of Foraminiferal

731   Research 34, 109–129.

732 Corliss, B.H., 1985. Microhabitat of benthic foraminifera with deep sea sediments. Nature 314,

733   435–438.

734 Corliss, B.H., 1991. Morphology and microhabitat preferences of benthic foraminifera from the

735   northwest Atlantic Ocean. Marine Micropaleontology 17, 195–236.

736 Corliss, B.H., Chen, C., 1988. Morphotype patterns of Norwegian deep sea benthic foraminifera

737   and ecological implications. Geology 16, 716–719.

738 Eicher, D.L., Worstell, P., 1970. Cenomanian and Turonian foraminfiera from the Great Plains,

739   United States. Micropaleontology 16, 269–324.

740 Erba, E., 2004. Calcareous nannofossils and Mesozoic oceanic anoxic events. Marine

741   Micropaleontology 52, 85–106.

742 Erba, E., Bottini, C., Faucher, G., 2013. Cretaceous large igneous provinces: The effects of

743   submarine volcanism on calcareous nannoplankton. Mineralogical Magazine 77, p. 1044.

744 Erbacher, J., Huber, B.T., Norris, R.D., Markey, M., 2001. Increased thermohaline stratification

745   as a possible cause for an ocean anoxic event in the Cretaceous period. Nature 409, 325–

746   327.

747   Farrimond, P., Eglinton, G., Brassell, S.C., 1990. The Cenomanian/Turonian anoxic event in

748   Europe: an organic geochemical study. Marine and Petroleum Geology 7, 75–89.

749   Fischer, A.G., Arthur, M.A., 1977. Secular variations in the pelagic realm. In: Cook, H.E. (ed.),

750   Deep-water carbonate environments. SEPM Sp. Pub. 25, 19–50.

751   Flores, J.A., Sierro, F.J., Filippelli, G.M., Barcena, M.A., Pérez-Folgado, M., Vázquez, A.,

752   Utrilla, R., 2005. Surface water dynamics and phytoplankton communities during

753   deposition of cyclic late Messinian sapropel sequences in the western Mediterranean.

754   Marine Micropaleontology 56, 50–79.

755   Föllmi, K.B., 1995. 160 m.y. record of marine sedimentary phosphorous burial: coupling of

756   climate and continental weathering under greenhouse and icehouse conditions. Geology 23,

757   859–862.

758   Fontanier, C., Jorissen, F.J., Licari, L., Alexandre, A., Anschutz, P., Carbonel, P., 2002. Live

759   benthic foraminiferal faunas from the Bay of Biscay: faunal density, composition and

760   microhabitats. Deep-Sea Research. Part 1. Oceanographic Research Papers 49, 751–785.

761   Friedrich, O., Erbacher, J., 2006. Benthic foraminiferal assemblages from Demerara Rise (ODP

762   Leg 207, western Tropical Atlantic): possible evidence for a progressive opening of the

763   Equatorial Atlantic Gateway. Cretaceous Research 27, 377–397.

764   Friedrich, O., Erbacher, J., Wilson, P.A., Moriya, K., Mutterlose, J., 2009. Paleoenvironmental

765   changes across the Mid Cenomanian Event in the tropical Atlantic Ocean (Demerara Rise,

766   ODP Leg 207) inferred from benthic foraminiferal assemblages. Marine Micropaleontology

767   71, 28–40.

768   Gallego-Torres, D., Martínez-Ruiz, F., Paytan, A., Jiménez-Espejo, F.J., Ortega-Huertas, M.,

769   2007. Pliocene–Holocene evolution of depositional conditions in the eastern Mediterranean:

770   Role of anoxia vs. productivity at 632 time of sapropel deposition. Palaeogeography,

771   Palaeoclimatology, Palaeoecology 246, 424–439.

772   Gavrilov, Y.O., Shcherbinina, E.A., Golovanova, O.V., Pokrovskii, B.G., 2013. The Late

773   Cenomanian paleoecological event (OAE 2) in the eastern Caucasus basin of Northern Peri-

774   Tethys. Lithology and Mineral Resources 48, 457–488.

775   Gebhardt, H., Kuhnt, W., Holbourn, A., 2004. Foraminiferal response to sea level change,

776   organic flux and oxygen deficiency in the Cenomanian of the Tarfaya Basin, southern

777   Morocco. Marine Micropaleontology 53, 133–157.

778   Gebhardt, H., Friederich, O., Schenk, B., Fox, L., Hart, M., Wagreich, M., 2010.

779   Paleoceanographic changes at the northern Tethyan margin during the Cenomanian-

780   Turonian Oceanic Anoxic Event (OAE2). Marine Micropaleontology 77, 25–45.

781   Gertsch, B., Keller, G., Adatte, T., Berner, Z., Kassab, A.S., Tantawy, A.A.A., El-Sabbagh,

782   A.M., Stueben, D., 2010. Cenomanian-Turonian transition in a shallow water sequence of

783   the Sinai, Egypt. International Journal of Earth Sciences 99, 165–182.

784   Gooday, A., 2003. Benthic foraminifera (Protista) as tools in deep-water palaeoceanography:

785   environmental influences on faunal characteristics. Advances in Biology 46, 1–90

786   Gupta, L.P., Kawahata, H., 2006. Downcore diagenetic changes in organic matter and

787   implications for paleoproductivity estimates. Global and Planetary Change 53, 122–136.

788   Gustafsson, M., Holbourn, A., Kuhnt, W., 2003. Changes in Northeast Atlantic temperature and

789   carbon flux during the Cenomanian/Turonian paleoceanographic event: the Goban Spur

790   stable isotope record. Palaeogeography, Palaeoclimatology, Palaeoecology 201, 51–66.

791   Hallam, A., 1992. Phanerozoic sea level changes. Columbia Press, New York, 266 pp.

792   Handoh, I.C., Lenton, T.M., 2003. Periodic mid-Cretaceous oceanic anoxic events linked by

793   oscillations of the phosphorous and oxygen biogeochemical cycles. Global Biogeochemical

794   Cycles 17, doi:10.1029/2003GB002039

795   Hardas, P., Mutterlose, M.J., 2007. Calcareous nannofossil assemblages of Oceanic Anoxic

796   Event 2 in the equatorial Atlantic: Evidence of an eutrophication event. Marine

797   Micropaleontology 66, 52–69.

798   Hardenbol, J., Thierry, J., Farley, M.B., Jacquin, T., de Graciansky, P.C., Vail, P.R., 1998.

799   Mesozoic and Cenozoic sequence chronostratigraphic framework of European Basins. In:

800   Graciansky, P.C., Hardenbol, J., Jacquin, T., Vail, P.R. (eds.), Mesozoic and Cenozoic

801   Sequence Stratigraphy of European Basins. SEPM Sp. Publ. 60, 3–13.

802   Hart, M.B., 1996. Recovery of the food chain after the late Cenomanian extinction event. In:

803   Hart, M.B. (ed.), Biotic recovery from Mass Extinction Events. Geological Society of

804   London Sp. Publ. 102, 265–277.

805   Hart, M.B., 1999. The evolution and diversity of Cretaceous planktonic foraminiferida. Geobios

806   32, 247–255.

807   Hart, M.B., Bailey, H.W., 1979. The distribution of planktonic Foraminiferida in the Mid-

808   Cretaceous of NW Europe. In: Wiedmann, J. (ed.), Aspekte der Kreide Europas.

809   International Union of Geological Sciences, Series A, 6, 527–542.

810   Hemleben, C., Spindler, M., Anderson, O.R., 1989. Modern planktonic foraminifera. Springer-

811   Verlag, Berlin, 363 pp.

812   Holbourn, A., Kuhnt, W., 2002. Cenomanian-Turonian palaeoceanographic change on the

813   Kerguelen Plateau a comparison with Northern Hemisphere records. Cretaceous Research

814   23, 333–349.

815   Holbourn, A., Kuhnt, W., Erbacher, J., 2001. Benthic foraminifers from lower Albian black

816   shales (Site 1049, ODP leg 171): evidence for a non 'uniformitarian' record. Journal of

817   Foraminiferal Research 31, 60–74.

818   Huber, B.T., Norris, R.D., McLeod, K.G., 2002. Deep-sea paleotemperature record of extreme

819   warmth during the Cretaceous. Geology 30, 123–126.

820   Ingall, E.D., Bustin, R.M., Van Cappellen, P., 1993. Influence of water column anoxia on the

821   burial and preservation of carbon and phosphorus in marine shales. Geochimica et

822   Cosmochimica Acta 57, 303–316.

823 Jarvis, I., Lignum, J.S., Groecke, D.R., Jenkyns, H.C., Pearce, M.A., 2011. Black shale

824   deposition, atmospheric CO2 drawdown, and cooling during the Cenomanian-Turonian

825   Oceanic Anoxic Event. Paleoceanography 26, PA3201.

826 Jones, R.W., Charnock, M.A., 1985. "Morphogroups" of agglutinating foraminifera. Their life

827   position and feeding habits and potential applicability in (paleo)ecological studies. Revue

828   Paléobiologie 4, 311–320.

829 Jones, B.A., Manning, D.A.C., 1994. Comparison of geochemical indices used for the

830   interpretation of paleoredox conditions in ancient mudstones. Chemical Geology 111, 111–

831   129.

832 Jorissen, F.J., De Stigter, H.C., Widmark, J.G.V., 1995. A conceptual model explaining benthic

833   foraminiferal habitats. Marine Micropaleontology 26, 3–15.

834 Kaiho, K., 1994. Planktonic and benthic foraminiferal extinction events during the last 100 m.y.

835   Palaeogeography, Palaeoclimatology, Palaeoecology 111, 45–71.

836 Kaiho, K., 1999. Evolution in the test size of deep-sea benthic foraminifera during the past 120

837   m.y. Marine Micropaleontology 37, 53–65.

838 Keller, G., Han, Q., Adatte, T., Burns, S.J., 2001. Paleoenvironment of the Cenomanian-

839   Turonian transition at Eastbourne, England. Cretaceous Research 22, 391–322.

840 Keller, G., Pardo, A., 2004. Age and environment of the Cenomanian-Turonian global

841   stratotype section and point at Pueblo, Colorado. Marine Micropaleontology 51, 95–128.

842 Klein, C., Mutterlose, J., 2001. Benthic foraminifera: indicators for a long-term improvement of

843   living conditions in the late Valanginian of the NW German Basin. Journal of

844   Micropalaeontology 20, 81–95.

845 Kuroda, J., Ogawa, N.O., Tanimizu, M., Coffin, M.T., Tokuyama, H., Kitazato, H., Ohkouchi,

846   N., 2007. Contemporaneous massive subaerial volcanism and late Cretaceous Oceanic

847   Anoxic Event 2. Earth Planetary Science Letters 256, 211–223.

848 Kuypers, M.M.M., Pancost, R.D., Nijenhuis, I.A., Sinninghe-Damste, J.S., 2002. Enhanced

849   productivity led to increased organic carbon burial in the euxinic North Atlantic Basin

850   during the late Cenomanian oceanic anoxic event. Paleoceanography 17, 1051.

851 Latimer, J.C., Filippelli, G.M., 2001. Terrigenous input and paleoproductivity in the Southern

852   Ocean. Paleoceanography 16, 627–643.

853 Leckie, R., Yuretich, R.F., West, O.L.O., Finkelstein, D., Schmidt, M., 1998. Paleoceanography

854   of the southwestern Western Interior Sea during the time of the Cenomanian-Turonian

855   boundary (Late Cretaceous). In: Dean, W., Arthur, M.A. (eds.) Stratigraphy and

856   Paleoenvironments of the Cretaceous Western Interior Seaway, USA. Society for

857   Sedimentary Geology, Concepts in Sedimentology and Paleontology 6, Tulsa, 101–126.

858 Leutenegger, S., Hansen, H.J., 1979. Ultrastructural and radiotracer studies of pore function in

859   foraminifera. Marine Biology 54, 11–16.

860 Monteiro, F.M., Pancost, R.D., Ridwell, A., Donnadieu, Y., 2012. Nutrients as the dominant

861   control on the spread of anoxia and euxinia across the Cenomanian-Turonian oceanic

862   anoxic event (OAE2): model-data comparison. Paleoceanography 27, PA4209.

863 Mort, M., Adatte, T., Föllmi, K.B., Keller, G., Steinmann, P., Matera, V., Berner, Z., Stüben,

864   D., 2007. Phosphorous and the roles of productivity and nutrient recycling during oceanic

865   event 2. Geology 35, 483–486.

866 Murray, J.W., 1991. Ecology and palaeoecology of benthic foraminifera. Longman, Harlow,

867   397 pp.

868 Nagao, S., Nakashima, S., 1992. Possible Complexation of Uranium with Dissolved Humic

869   Substances in Pore Water of Marine-Sediments. Science of the Total Environment 118,

870   439–447.

871 Nagy, J., 1992. Environmental significance of foraminiferal morphogroups in Jurassic North

872   Sea deltas. Palaeogeography, Palaeoclimatology, Palaeoecology 95, 111–134.

873   Nederbragt, A.J., Fiorentino, A., 1999. Stratigraphy and paleoceanography of the Cenomanian-

874   Turonian Boundary Event in Oued Mellegue, north-western Tunisia. Cretaceous Research

875   20, 47–62.

876   Negra, M.H., Zagrarni, M.F., Hanini, A., Strasser, A., 2011. The filament event near the

877   Cenomanian-Turonian boundary in Tunisia: filament origin and environmental

878   signification. Bulletin Société Géologique France 182, 507–519.

879   Norris, R.D., Bice, K.L., Magno E.A., Wilson, P.A., 2002. Jiggling the tropical thermostat in

880   the Cretaceous hothouse. Geology 30, 299–302.

881   Peryt, D., 2004. Benthic foraminiferal response to the Cenomanian-Turonian and Cretaceous-

882   Paleogene boundary events. Przegląd Geologiczny 52, 827–832.

883   Peryt, D., Lamolda, M., 1996. Benthonic foraminiferal mass extinction and survival

884   assemblages from the Cenomanian-Turonian Boundary Event in the Menoyo section,

885   northern Spain. Geological Society, London, Special Publications 102, 245–258.

886   Petrizzo, M.R., 2002. Palaeoceanographic and palaeoclimatic inferences from Late Cretaceous

887   planktonic foraminiferal assemblages from the Exmouth Plateau (ODP Sites 762 and 763,

888   eastern Indian Ocean). Marine Microplaeontology 45, 117–150.

889   Plewa, K., Meggers, H., Kasten, S., 2006. Barium in sediments off northwest Africa: A tracer

890   for palaeoproductivity or meltwater events? Paleoceanography 21, PA2015.

891   Pogge von Strandmann, P.A.E., Jenkyns, H.C., Woodfine, R.G., 2013. Lithium isotope evidence

892   for enhanced weathering during Oceanic Anoxic Event 2. Nature Geoscience 6, 668–672.

893   Powell, W.G., Johston, P.A., Collom, C.J., 2003. Geochemical evidence for oxygenated bottom

894   waters during deposition of fossiliferous strata of the Burgess Shale Formation.

895   Palaeogeography, Palaeoclimatology, Palaeoecology 201, 249–268.

896   Premoli Silva, I., Sliter, W.V., 1999. Cretaceous Paleoceanography: evidence from planktonic

897   foraminiferal evolution. In: Barrera, E., Johnson C.C. (eds.), Evolution of the Cretaceous

898   Ocean-Climate System. Geological Society America Sp Paper 332, 301–328.

899   Reolid, M., Martínez-Ruiz, F., 2012. Comparison of benthic foraminifera and geochemical

900   proxies in shelf deposits from the Upper Jurassic of the Prebetic (southern Spain). Journal of

901   Iberian Geology 38, 449–465.

902   Reolid, M., Rodríguez-Tovar, F.J., Nagy, J., Olóriz, F., 2008. Benthic foraminiferal

903   morphogroups of mid to outer shelf environments of the Late Jurassic (Prebetic Zone,

904   Southern Spain): Characterisation of biofacies and environmental significance.

905   Palaeogeography, Palaeoclimatology, Palaeoecology 261, 280–299.

906   Reolid, M., Rodríguez-Tovar, F.J., Marok, A., Sebane, A., 2012a. The Toarcian Oceanic

907   Anoxic Event in the Western Saharan Atlas, Algeria (North African Paleomargin): role of

908   anoxia and productivity. Geological Society of America Bulletin 124, 1646–1664.

909   Reolid, M., Rodríguez-Tovar, F.J., Nagy, J., 2012b. Ecological replacement of Valanginian

910   agglutinated foraminifera during a maximum flooding event in the Boreal realm

911   (Spitsbergen). Cretaceous Research 33, 196–204.

912   Robaszynski, F., Caron, M., Amédro, F., Dupuis, C., Hardenbol, J., González-Donoso, J.M.,

913   Linares, D., Gartner, S., 1993. Le Cénomanien de la región de Kalaat Senan (Tunisie

914   Centrale): Litho-biostratigraphie et interprétation séquentielle. Revue de Paléobiologie 12,

915   351–505.

916   Robaszynski, F., Caron, M., Dupuis, C., Amédro, F., González-Donoso, J.M., Linares, D.,

917   Hardenbol, J., Gartner, S., Calandra, F., Deloffre, 1990. A tentative integrated stratigraphy

918   in the Turonian of central Tunisia: Formations, zones and sequential stratigraphy in the

919   Kalaat Senan area. Bull. Centre Recherche Exploration-Production Elf-Aquitaine 14, 213–

920   384.

921   Robaszynski, F., Zargrani, M.F., Caron, M., Amédro, F., 2010. The global bio-events at the

922   Cenomanian-Turonian transition in the reduced Bahloul Formation of Bou Ghanem

923   (central Tunisia). Cretaceous Research 31, 1-15.

924 Robertson, A.K., Filippelli, G.M., 2008. Paleoproductivity variations in the eastern equatorial

925 Pacific over glacial timescales: American Geophysical Union Fall Meeting 2008, Abstract

926 PP33C-1576.

927 Saïdi, F., Ben Ismaïl, M.H., M'Rabat, A., 1997. Le Turonien de Tunisie centro-occidentale:

928 facies, paléogéographie séquentielle d'une plate-form. Cretaceous Research 18, 63–85.

929 Sarmiento, J.L., Herbert, T.D., Toggweiler, J.R., 1988. Causes of anoxia in the world ocean.

930 Global Biogechemical Cycles 2, 115–128.

931 Schlanger, S.O., Jenkyns, H.C., 1976. Cretaceous oceanic anoxic events, causes and

932 consequences. Geologie en Mijnbouw 55, 179–184.

933 Schlanger, S.O., Arthur, M.A., Jenkyns, H.C., Scholle, P.A., 1987. The Cenomanian-Turonian

934 oceanic anoxic event, I. Stratigraphy and distribution of organic-rich beds and the marine

935 $\delta^{13}C$ excursión. In: Brooks, J., Fleet, A.J. (eds.), Marine Petroleum Source Rocks. Special

936 Publication, Geol. Soc. London 26, 371–399.

937 Scholle, P.A., Arthur, M.A., 1980. Carbon isotope fluctuations in Cretaceous pelagic

938 limestones: potential stratigraphic and petroleum exploration tool. AAPG Bulletin 64, 67–

939 87.

940 Scopelliti, G., Bellanca, A., Coccioni, R., Luciani, V., Neri, R., Baudin, F., Chiari, M.,

941 Marcucci, M., 2004. High-resolution geochemical and biotic records of the Tethyan

942 'Bonarelli Level' (OAE2, latest Cenomanian) from the Calabianca-Guidaloca composite

943 section, northwestern Sicily, Italy. Palaeogeography, Palaeoclimatology, Palaeoecology

944 208, 293–317.

945 Scott, R.W., 2003. High resolution North African Cretaceous stratigraphy: status. In: Gili, E.,

946 Negra, M.H., Skelton, W. (Eds.), Cretaceous carbonate platform systems. Nato Science

947 Series 28, 1–17.

948 Sen, A.K., Filippelli, G.M., Flores, J.A., 2008. An application of wavelet analysis to

949 palaeoproductivity records from the Southern Ocean. Computers & Geosciences 35, 1445–

950 1450.

951 Sliter, W.V., 1975. Foraminiferal life and residue assemblages from Cretaceous slope deposits.

952   Geological Society of America Bulletin 86, 897–906.

953 Soua, M., Zaghbib-Turki, D., Ben Jemia, H., Smaoui, J., Boukadi, A., 2011. Geochemical

954   Record of the Cenomanian-Turonian Anoxic Event in Tunisia: Is it Correlative and

955   Isochronous to the Biotic Signal? Acta Geologica Sinica 85, 801–840.

956 Sprong, J., Kouwenhoven, T.J., Bornemann, A., Dupuis, C., Speijer, R.P., Stassen, P.,

957   Steurbaut, E., 2013. In search of the Latest Danian Event in a paleobathymetric transect off

958   Kasserine Island, north-central Tunisia. Palaeogeography Palaeoclimatology Palaeoecology

959   379, 1–-16.

960 Su, W., Wang, Y., Cramer, B.D., Munnecke, A., Li, Z., Fu, L., 2008. Preliminary estimation of

961   palaeoproductivity via TOC and habitat types: which method is more reliable? A case

962   study on the Ordovician/Silurian transitional black shales of the Upper Yangtze Platform,

963   South China. Journal of China University of Geosciences 19, 534–548.

964 Sun, Y.B., Wu, F., Clemens, S.C., Oppo, D.W., 2008. Processes controlling the geochemical

965   composition of the South China Sea sediments during the last climatic cycle. Chemical

966   Geology 257, 234–249.

967 Thierry, J., 2000. Middle Callovian (157–155 Ma). In: Dercourt, J., Gaetani, M., Vrielynck, B.,

968   Barrier, E., Biju-Duval, B., Brunet, M-F., Cadet, J.P., Crasquin, S., Sandulescu, M. (Eds.),

969   Atlas Peri-Tethys palaeogeographical maps. CCGM/CGMW, Paris, pp. 71–97.

970 Tribovillard, N., Algeo, T., Lyons, T., Riboulleau, A., 2006. Trace metals as palaeoredox and

971   palaeoproductivity proxies: an update. Chemical Geology 232, 12–32.

972 Trivobillard, N., Algeo, T.J., Baudin, F., Riboulleau, A., 2012. Analysis of marine

973   environmental conditions based on molybdenum-uranium covariation – Applications to

974   Mesozoic paleoceanography. Chemical Geology 324–325, 46–58.

975 Tsandev, I., Slomp, C.P., 2009. Modeling phosphorous cycling and carbon burial during

976   Cretaceous Oceanic Anoxic Events. Earth and Planetary Science Letters 286, 71–79.

977   Turgeon, S.C., Brumsack, H.J., 2006. Anoxic vs dysoxic events reflected in sediment

978   geochemistry during the Cenomanian-Turonian Boundary Event (Cretaceous) in the

979   Umbria-Marche basin of central Italy. Chemical Geology 234, 321–339.

980   Turgeon, S.C., Creaser, R.A., 2008. Cretaceous oceanic anoxic event 2 triggered by a massive

981   magmatic episode. Nature 454, 323–326.

982   Tyszka, J., 1994. Response of Middle Jurassic benthic foraminiferal morphogroups to

983   dysoxic/anoxic conditions in the Pieniny Klippen Basin, Polish Carpathians.

984   Palaeogeography, Palaeoclimatology, Palaeoecology 110, 55–81.

985   Valentine, J.W., 1973. Evolutionary ecology of the marine biosphere. Prentice Hall, Englewood

986   NJ, 511 pp.

987   Van Cappellen, P., Ingall, E.D., 1994. Benthic phosphorus regeneration, net primary production,

988   and ocean anoxia—A model of the coupled marine biogeochemical cycles of carbon and

989   phosphorus. Paleoceanography 9, 677–692.

990   Van der Zwaan, G.J., Duijnstee, I.A.P., Den Dulk, M., Ernst, S.R., Jannink N.T., Kouwenhoven,

991   T.J., 1999. Benthic foraminifers: proxies or problem? A review of paleoecological

992   concepts. Earth-Science Reviews 46, 213–236.

993   Wagner, T., Wallmann, K., Herrle, J.O., Hofmann, P., Stuesser, L., 2007. Consequences of

994   moderate 25,000 yr lasting emission of light CO2 into the mid-Cretaceous ocean. Earth

995   Planetary Science Letters 259, 200–211.

996   Wang, C.S., Hu, X.M., Jansa, L., Wan, X.Q., Tao, R., 2001. The Cenomanian-Turonian anoxic

997   event in southern Tibet. Cretaceous Research 22, 481–490.

998   Widmark, J.G.V., Speijer, R.P., 1997. Benthic foraminiferal faunas and trophic regimes at the

999   terminal Cretaceous Tethyan seafloor. Palaios 12, 354–371.

1000   Wignall, P.B., Myers, K.J., 1988. Interpreting the benthic oxygen levels in mudrocks: a new

1001   approach. Geology 16, 452–455.

1002 Zaghbib-Turki, D., Soua, M., 2013. High resolution biostratigraphy of the Cenomanian-

1003   Turonian interval (OAE2) based on planktonic foraminiferal bioevents in North-Central

1004   Tunisia. Journal of African Earth Sciences 78, 97–108.

1005 Zagrarni, M.F., Negra, M.H., Hanini, A., 2008. Cenomanian-Turonian facies and sequence

1006   stratigraphy, Bahloul Formation, Tunisia. Sedimentary Geology 204, 18–35.

1007 Zheng, X.Y., Jenkyns, H.C., Gale, A.S., Ward, D.J., Henderson, G.M., 2013. Changing ocean

1008   circulation and hydrothermal inputs during Ocean Anoxic Event 2 (Cenomaian-Turonian):

1009   Evidence from Nd-isotopes in the European shelf sea. Earth and Planetary Science Letters

1010   375, 338–348.

1011 Zhou, L., Wignall, P.B., Su, J., Feng, Q., Xie, S., Zhao, L., Huang, J., 2012. U/Mo ratios and

1012 $\delta^{98/95}$Mo as local and global redox proxies during mass extinction events. Chemical

1013   Geology 324-325, 99–197.

1014

Appendix 1: Planktic foraminiferal species

Anaticinella multiloculata (Morrow, 1934)

Dicarinella algeriana (Caron, 1966)

Dicarinella hagni (Scheibnerova, 1962)

Dicarinella imbricata (Mornod, 1950)

Globigerinelloides bentonensis (Morrow, 1934)

Globigerinelloides ultramicrus (Subbotina, 1949)

Globoheterohelix paraglobulosa Georgescu and Huber, 2009

Guembelitria cenomana (Keller, 1935)

Hedbergella delrioensis (Carsey, 1926)

Hedbergella planispira (Tappan, 1940)

Hedbergella simplex (Morrow, 1934)

Helvetoglobotruncana helvetica (Bolli, 1945)

Helvetoglobotruncana praehelvetica (Trujillo, 1960)

1029   *Heterohelix moremani* (Cushman, 1938)

1030   *Heterohelix pulchra* (Brotzen, 1936)

1031   *Heterohelix reussi* (Cushman, 1938)

1032   *Praeglobotruncana gibba* Klaus, 1960

1033   *Praeglobotruncana stephani* (Gandolfi, 1942)

1034   *Rotalipora cushmani* (Morrow, 1934)

1035   *Rotalipora monsalvensis* (Mornod, 1950)

1036   *Shackoina bicornis* (Reichel, 1948)

1037   *Schackoina cenomana* (Shacko, 1897)

1038   *Thalmanninella brotzeni* (Sigal, 1948)

1039   *Thalmanninella greenhornensis* (Morrow, 1934)

1040   *Whiteinella aprica* (Loeblich and Tappan, 1961)

1041   *Whiteinella archaeocretacea* Pesaggno, 1967

1042   *Whiteinella aumalensis* (Sigal, 1952)

1043   *Whiteinella baltica* Douglas and Rankin, 1969

1044   *Whiteinella brittonensis* (Loeblich and Tappan, 1961)

1045   *Whiteinella paradubia* (Sigal, 1952)

1046   *Whiteinella* sp.

1047

1048   **Appendix 2: Benthic foraminiferal species**

1049   *Ammodiscus* spp.

1050   *Arenobulimina* spp.

1051   *Astacolus* spp.

1052   *Bathysiphon* spp.

1053   *Bigenerina* sp.

1054   *Bolivina* sp.

1055   *Bolivinopsis* sp.

1056   *Brunsvigella thoerensis* (Bartenstein and Brand, 1951)

1057   *Charltonina australis* Scheibnerová, 1978

1058   *Charltonina* sp.

1059   *Conorotalites* sp.

1060   *Coryphostoma* spp.

1061   *Dorothia pupa* (Reuss, 1860)

1062   *Dorothia* spp.

1063   *Frondicularia* sp.

1064   *Gaudryina pyramidata* Cushman, 1926

1065   *Gaudryina* spp.

1066   *Gavelinella barremiana* Bettenstaedt, 1952

1067   *Gavelinella cenomanica* (Brotzen, 1945)

1068   *Gavelinella flandrini* Moullade. 1960

1069   *Gavelinella intermedia* (Berthelin, 1880)

1070   *Gavelinella rochardensis* Beckmann, 1991

1071   *Gavelinella* spp.

1072   *Glandulina* sp.

1073   *Globorotalites* sp.

1074   *Globulina* spp.

1075   *Gyroidinoides beisseli* (White, 1928)

1076   *Gyroidinoides globosus* (Hagenow, 1842)

1077   *Gyroidinoides lenticulus* (Reuss, 1845)

1078   *Gyroidinoides* spp.

1079   *Gyroidinoides subglobosus* Dailey, 1970

1080   *Laevidentalina* spp.

1081   *Lagena* spp.

1082   *Lenticulina gaultina* (Berthelin, 1880)

1083   *Lenticulina* spp.

1084   *Lenticulina subgaultina* Bartenstein, 1962

1085   *Lingulina* sp.

1086   *Lingulina taylorana* Cushman, 1938

1087   *Lingulogavelinella frankei* (Bykova, 1953)

1088   *Lingulogavelinella* sp.

1089   *Marssonella oxycona* (Reuss, 1860)

1090   *Neobulimina albertensis* (Stelck and Wall, 1954)

1091   *Neobulimina irregularis* Cushman and Parker, 1936

1092   *Neobulimina* spp.

1093   *Neobulimina subregularis* (de Klasz, Magné and Rérat, 1963)

1094   *Neoflabellina* sp.

1095   *Palmula* sp.

1096   *Planularia advena* Cushman and Jarvis, 1932

1097   *Planularia dissona* Plummer, 1931

1098   *Planularia* sp.

1099   *Praebulimina* cf. *exigua* Cushman and Parker, 1935

1100   *Praebulimina nannina* (Tappan, 1940)

1101   *Praebulimina reussi* (Morrow, 1934)

1102   *Praebulimina* spp.

1103   *Pyrulina* spp.

1104   *Pyrulinoides* spp.

1105   *Quadrimorphina* sp.

1106   *Quasispiroplectammina* spp.

1107   *Ramulina* spp.

1108   *Reophax* sp.

1109   *Repmanina charoides* (Jones and Parker, 1860)

1110   *Saracenaria* sp.

1111   *Spiroplectammina* sp.

1112   *Stensioeina exsculpta* (Reuss, 1860)

1113   *Tappanina laciniosa* Eicher and Worstell, 1970

1114   *Tappanina* sp.

1115   *Textularia* sp.

1116   *Trochammina globolaevigata* Beckmann, 1991

1117   *Vaginulina* sp.

1118   *Valvulineria* sp.

1119

1120

1121

1122   **Figure caption.**

1123

1124   **Fig. 1.** (A) Geological setting, (B) palaeogeographic reconstruction of Western Tethys after

1125   Thierry (2000) and (C) Oued Bahloul section. Ammonite biostratigraphy according to

1126   Caron et al. (1999, 2006), Accarie et al. (2000), Amédro et al. (2005) and Zagrarni et al.

1127   (2008).

1128   **Fig. 2.** Planktic foraminiferal species in the Oued Bahloul section: **1-** *Globigerinelloides*

1129   *bentonensis* (OB-3.5). **2-** *Globoheterohelix paraglobulosa* (OB-42). **3-** *Guembelitria*

1130   *cenomana* (OB-24). **4-** *Hedbergella delrioensis* (OB-42). **5-** *Hedbergella planispira* (OB-

1131   22). **6-** *Hedbergella simplex* (OB-3). **7-8** *Helvetoglobotruncana helvetica* (7: OB-44, 8: OB-

1132   35). **9-** *Heterohelix moremani* (OB-13). **10-** *Heterohelix reussi* (OB-22). **11-**

1133   *Praeglobotruncana gibba* (OB-3). **12-** *Praeglobotruncana stephani* (OB-3.5). **13-**

1134   *Rotalipora cushmani* (OB-3). **14-** *Rotalipora brotzeni* (OB-3.5). **15-** *Rotalipora*

1135   *greenhornensis* (OB-3.5). **16-** *Whiteinella archaeocretacea* (OB-20). **17-** *Whiteinella aprica*

1136   (OB-37). **18** *Whiteinella brittonensis* (OB-28). Scale bars: 0.1 mm.

1137 **Fig. 3.** Benthic foraminiferal species in the Oued Bahloul section: **1-** *Neobulimina albertensis*

1138 (OB-10). **2-** *Neobulimina subregularis* (OB-10). **3-** *Praebulimina prolixa* (OB-24). **4-**

1139 *Lenticulina gaultina* (OB-2). **5-** *Gyroidinoides lenticulus* (OB-2). **6-** *Gyroidinoides globosus*

1140 (OB-2). **7-** *Praebulimina nannina* (OB-2). **8-** *Gaudryina pyramidata* (OB-3). **9-**

1141 *Marssonella oxycona* (OB-3). **10-** *Lenticulina* sp (OB-3). **11-** *Trochammina globolaevigata*

1142 (OB-3). **12-** *Praebulimina* sp (OB-8). **13-** *Praebulimina reussi* (OB-8). **14-** *Gavelinella*

1143 *rochardensis* (OB-8). **15-** *Planularia advena* (OB-35.5). **16-***Tappanina laciniosa* (OB-33).

1144 **17-** *Gavelinella* cf. *rochardensis* (OB-22). **18-** *Astacolus* ? sp. (OB-35). Scale bars: 0.1 mm

1145 **Fig. 4.** Stratigraphic distribution of planktic/benthic ratio and diversity of planktic and benthic

1146 foraminifera.

1147 **Fig. 5.** Stratigraphic distribution of planktic foraminiferal assemblages.

1148 **Fig. 6.** Stratigraphic distribution of benthic foraminiferal assemblages.

1149 **Fig. 7.** Stratigraphic fluctuations of geochemical redox proxies and U- and Mo-based proxies

1150 (enrichment factor and authigenic content).

1151 **Fig. 8.** Stratigraphic fluctuations of CO_3Ca content, TOC and geochemical palaeproductivity

1152 proxies.

1153 **Fig. 9.** Stratigraphic fluctuations of $\delta^{13}C$ and $\delta^{18}O$ and comparison with previous $\delta^{13}C$ curves of

1154 Caron et al. (2006) (dashed line) and Zagrarni et al. (2008) (dotted line).

1155 **Fig. 10.** Evolution of trophic conditions, productivity and oxygenation in the water column and

1156 the seafloor (sea-bottom waters) inferred from foraminiferal assemblages and geochemical

1157 proxies.

1158

1159

1160 **Table caption**

1161 Table 1. Planktic foraminiferal counts per sampling level.

1162 Table 2. Benthic foraminiferal counts per sampling level.

1163   Table 3. Planktic forms and inferred life style including redox and trophic requirements of

1164   planktic foraminifera from Ouled Bahloul section based on Hart and Bailey (1979), Hart

1165   (1999), Keller et al. (2001) and Coccioni and Luciani (2005).

Figure 01
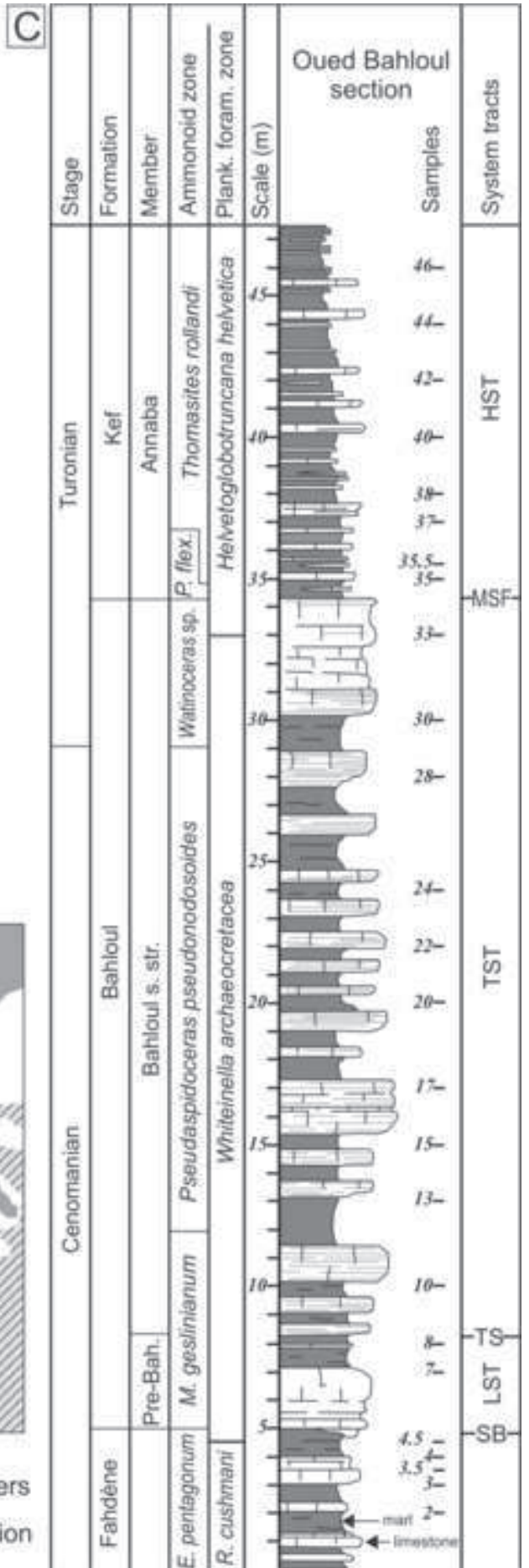[Click here to download high resolution image](#)
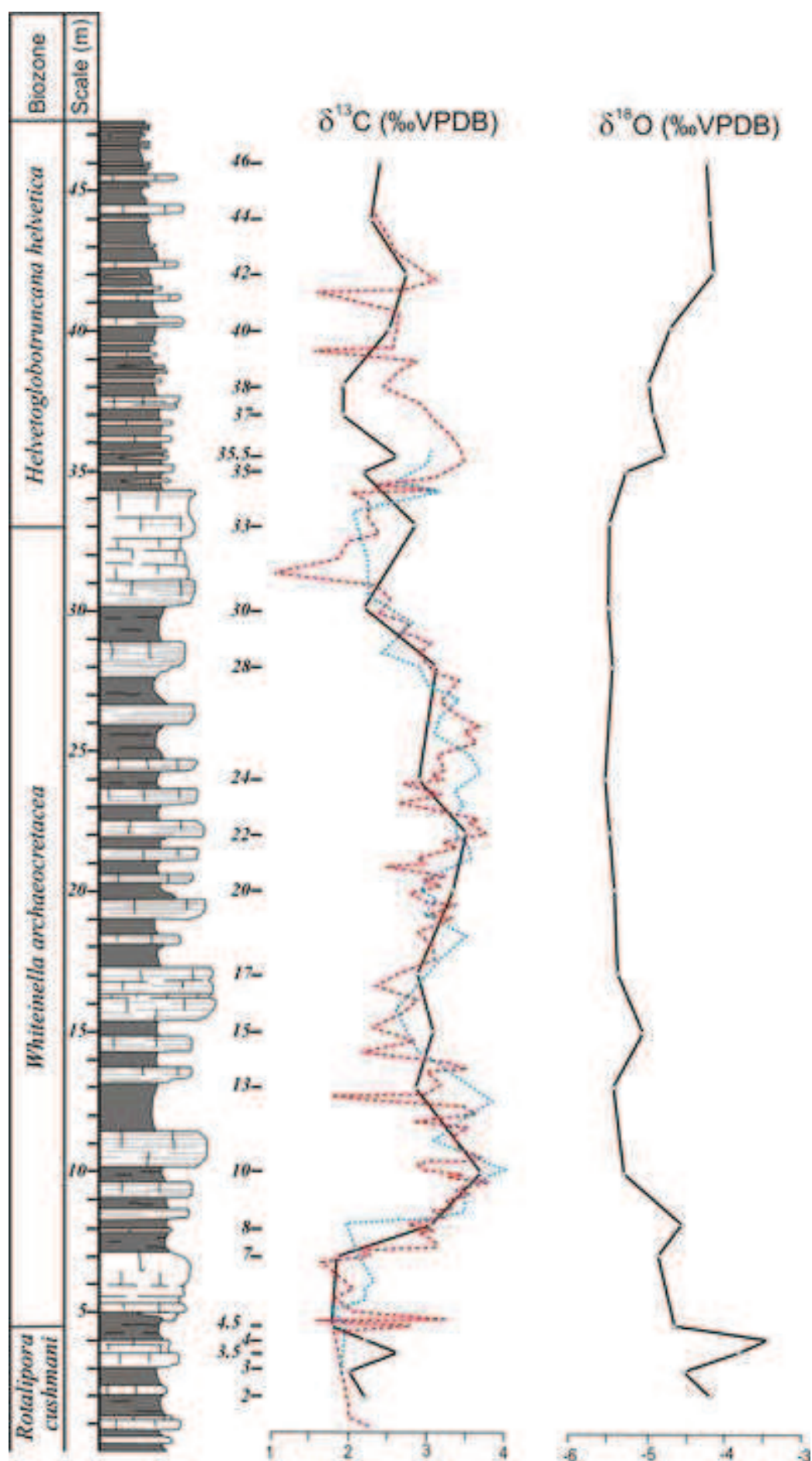
Figure 03
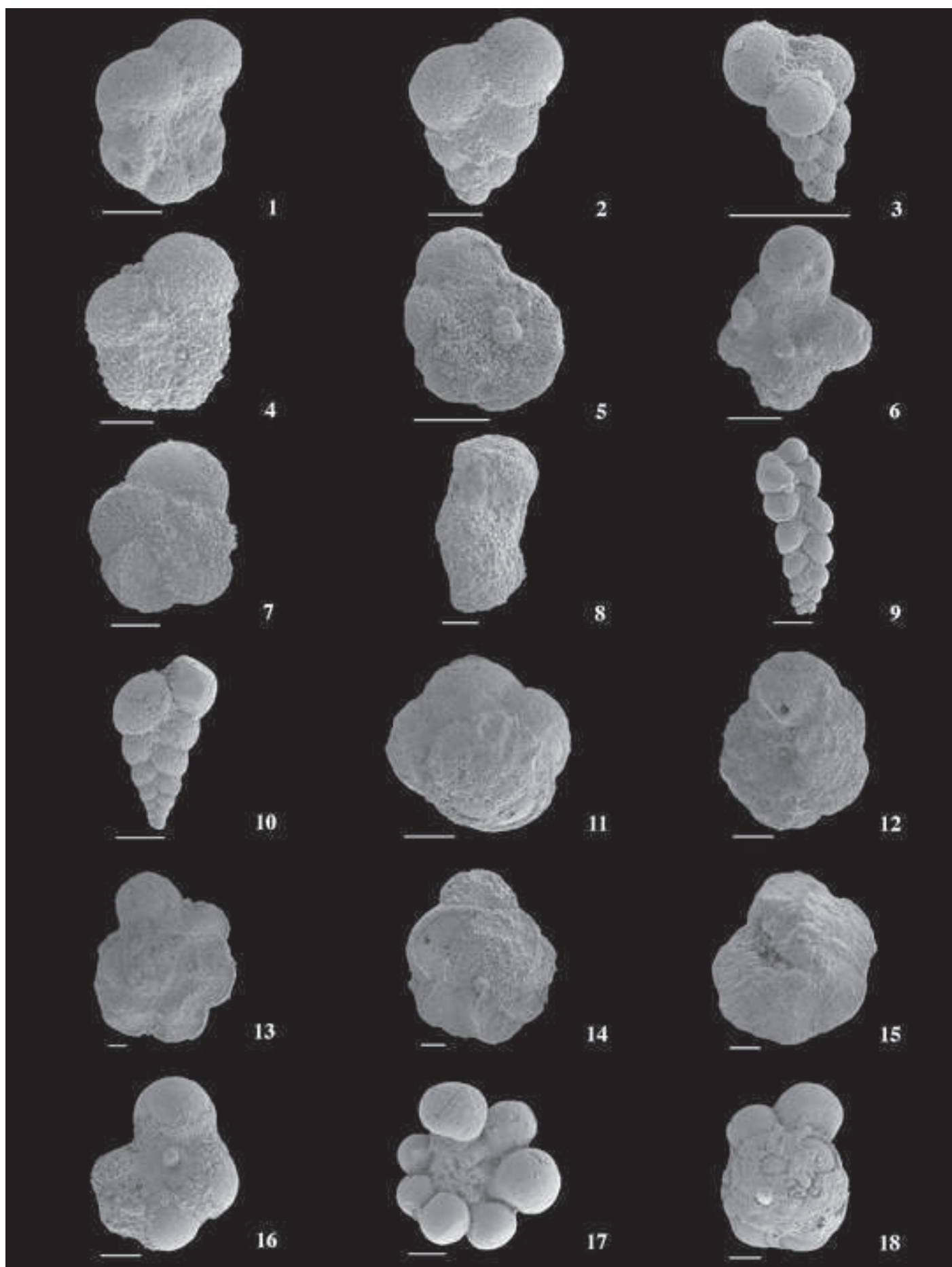Click here to download high resolution image

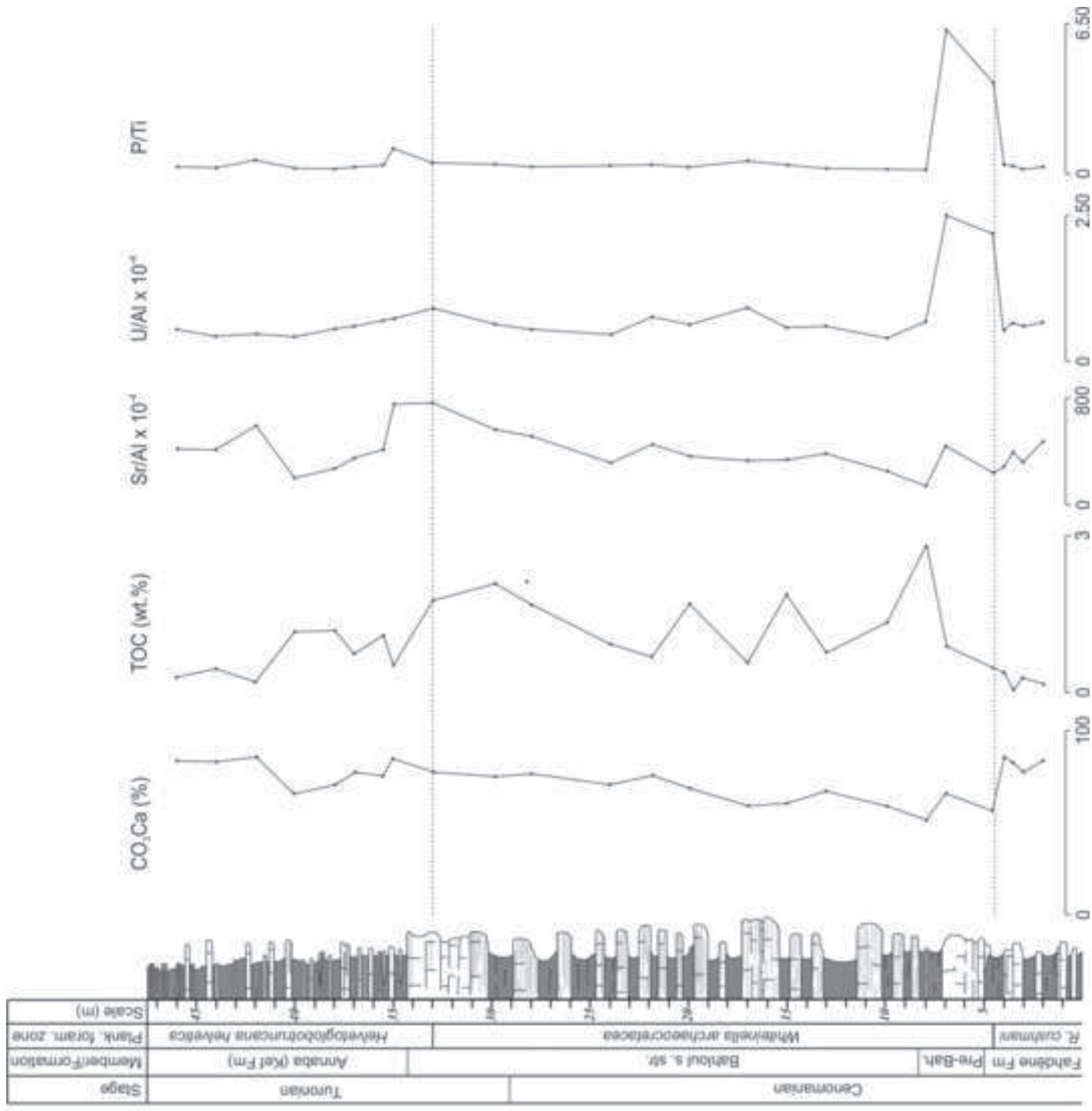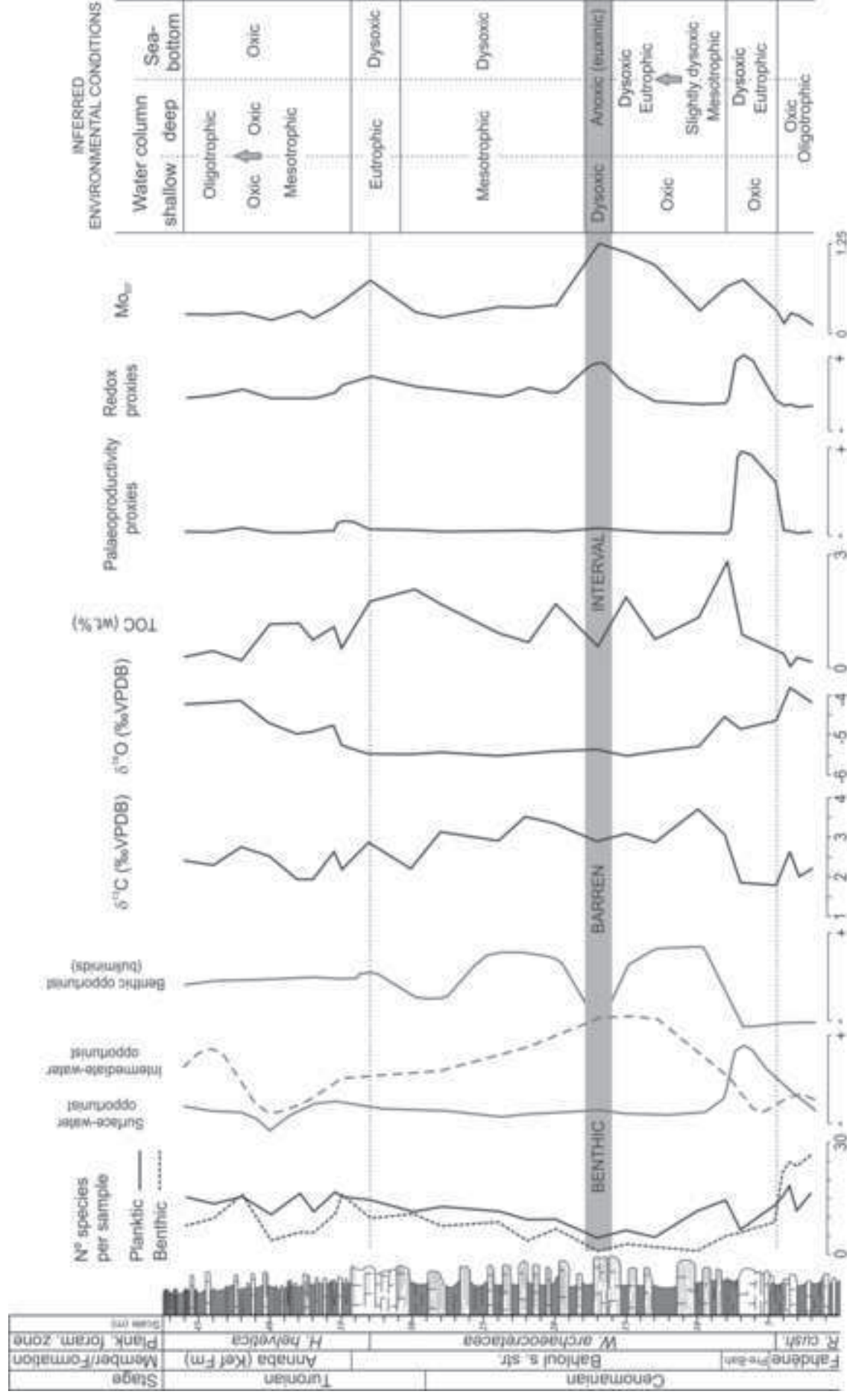**Table 01**

SAMPLE	Anaticinella multiloculata	Dicarinella algeriana	Dicarinella hagni	Dicarinella imbricata	Globigerinelloides bentonensis	Globigerinelloides ultramicrus	Globoheterohelix paraglobulosa	Guembelitria cenomana	Hedbergella delrioensis	Hedbergella planispira	Hedbergella simplex	Helvetoglobotruncana helvetica	Helvetoglobotruncana praehelvetica	Heterohelix moremani
OB10-46	0	4	0	0	0	0	26	0	82	19	4	1	26	6
OB10-44	0	3	0	0	0	0	66	6	19	8	1	0	13	4
OB10-42	0	5	0	0	0	0	37	17	57	5	3	3	11	0
OB10-40	0	0	0	0	0	0	3	0	0	0	0	1	2	0
OB10-38	0	3	1	0	0	0	10	21	41	38	3	8	11	4
OB10-37	0	0	0	0	0	0	15	0	31	7	5	25	22	0
OB10-35.5	0	0	0	0	0	0	20	68	73	17	17	3	2	4
OB10-35	0	5	3	1	0	0	19	25	61	15	0	7	20	3
OB10-33	0	1	2	0	0	0	27	70	21	19	0	3	15	2
OB10-30	0	0	0	0	0	0	32	8	25	17	0	0	10	5
OB10-28	0	0	0	0	2	0	0	7	22	23	0	0	7	1
OB10-24	0	0	0	0	0	0	0	4	4	20	0	0	23	8
OB10-22	0	0	0	0	0	0	0	7	14	27	0	0	2	38
OB10-20	0	0	0	0	0	0	0	12	7	35	0	0	18	13
OB10-17	0	0	0	0	0	0	0	0	4	10	0	0	0	1
OB10-15	0	0	0	0	0	0	1	2	4	30	0	0	0	18
OB10-13	0	0	0	0	0	0	0	0	4	40	4	0	0	35
OB10-10	0	0	0	0	0	0	11	0	17	21	0	0	3	10
OB10-8	0	0	0	0	3	2	0	14	89	22	12	0	1	4
OB10-7	0	0	0	0	1	1	0	0	22	1	0	0	0	0
OB10-4.5	0	0	0	0	14	1	0	0	57	27	5	0	0	0
OB10-4	0	0	0	0	47	3	0	0	143	12	17	0	0	3
OB10-3.5	1	1	0	0	78	8	0	0	90	25	25	0	0	3
OB10-3	0	0	0	0	80	16	0	0	42	123	34	0	0	5
OB10-2	0	0	1	0	32	31	0	5	89	80	38	0	0	6

Table 02

SAMPLE \ SPECIES	Ammodiscus spp.	Arenobulimina spp.	Astacolus spp.	Bathysiphon spp.	Bigenerina sp.	Bolivina sp.	Bolivinopsis sp.	Brunsvigella thoerensis	Charltonina australis	Charltonina sp.	Conorotalites sp.	Coryphostoma spp.	Dorothia pupa	Dorothia spp.	Frondicularia sp.	Gaudryina pyramidata
OB10-46	0	0	0	0	0	0	0	0	0	0	0	0	0	0	1	0
OB10-44	0	0	0	0	0	0	0	0	0	0	0	1	0	0	0	0
OB10-42	0	1	0	0	0	1	0	0	0	0	0	0	0	0	0	0
OB10-40	0	0	0	0	0	0	0	0	0	0	0	0	0	0	0	0
OB10-38	0	0	0	0	0	0	0	0	0	0	0	0	0	0	0	0
OB10-37	0	0	0	0	0	2	0	0	0	0	0	0	0	0	0	0
OB10-35.5	0	0	0	0	0	0	0	0	0	0	0	0	0	0	0	0
OB10-35	0	0	5	0	0	4	0	0	0	0	0	4	0	6	2	0
OB10-33	0	0	0	1	0	3	0	0	0	0	0	0	0	0	0	0
OB10-30	0	0	0	0	0	2	0	0	0	0	0	1	0	0	0	0
OB10-28	0	0	0	0	0	0	0	0	0	0	0	0	0	0	0	0
OB10-24	0	0	0	0	1	0	0	0	0	0	0	0	0	0	0	0
OB10-22	0	0	0	0	0	0	0	0	0	0	0	0	0	0	0	0
OB10-20	0	0	0	0	0	0	0	2	0	0	0	0	0	0	0	0
OB10-17	0	0	0	0	0	0	0	0	0	0	0	0	0	0	0	0
OB10-15	0	0	0	0	0	0	0	0	0	0	0	0	0	0	0	0
OB10-13	0	0	0	0	0	0	0	0	0	0	0	9	0	0	0	0
OB10-10	0	0	0	0	0	0	0	0	0	0	0	0	0	0	0	0
OB10-8	0	0	2	0	0	0	0	0	0	0	0	1	0	0	0	0
OB10-7	0	0	0	0	0	0	0	0	0	0	0	0	0	0	0	0
OB10-4.5	0	0	1	0	0	0	0	0	0	0	0	0	0	0	1	0
OB10-4	1	0	1	0	0	0	0	0	7	0	1	14	0	2	0	0
OB10-3.5	2	0	0	1	0	0	2	0	1	0	3	1	0	4	0	2
OB10-3	0	0	0	0	0	0	0	0	0	0	3	8	3	2	0	2
OB10-2	1	0	0	0	0	0	0	0	2	1	3	0	2	1	0	0

Table 03
Click here to download Table: Table 3.xls

Morphology	Genera	Habitat	Mode
Strongly keeled trochospiral	*Dicarinella*	Intermediate-dweller	Intermediate
	Rotalipora	Intermediate to deep-	Specialist
	Thalmanninella	Intermediate to deep-	Specialist
Weakly keeled trochospiral	*Anaticinella*	Intermediate-dweller	Intermediate
	Helvetoglobotruncana	Intermediate to deep-dweller	Intermediate to specialist
	Praeglobotruncana	Intermediate-dweller	Intermediate
Unkeeled trochospiral	*Hedbergella*	Surface-dweller	Opportunist
	Shackoina	Intermediate-dweller	Intermediate
	Whiteinella	Surface-dweller	Opportunist
Planispiral	*Globigerinelloides*	Surface to intermediate-dweller	Opportunist to Intermediate
Biserial	*Heterohelix*	Surface to intermediate -dweller	Opportunist
Triserial	*Guembelitria*	Surface-dweller	Opportunist